Rhizosphere water content drives hydraulic redistribution :
Implications of pore-scale heterogeneity to modeling diurnal
transpiration in water-limited ecosystems

Montaldo, Nicola

2022-01-15

Rhizosphere water content drives hydraulic redistribution: Implications of pore-scale heterogeneity to modeling diurnal transpiration in water-limited ecosystems

Nicola Montaldo [a,*], Ram Oren [b,c,*]

[a] Dipartimento di Ingegneria civile, ambientale e architettura, Università di Cagliari, Via Marengo, 3, I-09123, Italy
[b] Nicholas School of the Environment & Pratt School of Engineering, Duke University, Durham, NC 27708, United States of America
[c] Department of Forest Science, University of Helsinki, Finland

ARTICLE INFO

ABSTRACT

Trees typically survive prolonged droughts by absorbing water from deeper layers. Where soils are shallow, roots may be extract water from the underlying fractured bedrocks. In dry seasons, surface-soil moisture dynamics reflect hydraulic redistribution (HR). HR is usually estimated based on the gradient of mean, or bulk, soil water potential among layers in the rooting zone (HR_B). This approach neglects the potential effect of spatial heterogeneity of water content at the millimeter scale between the rhizosphere and bulk soil. We proposed to account for the rhizosphere water balance, estimating HR to the rhizosphere (HR_R) of the dry surface soil from the underlying fractured rock. The model was evaluated using a 15-year dataset collected in Sardinia. When the typical approach, based on moisture gradients among bulk soil layers, was used for estimating HR_B, tree transpiration was underpredicted in all seasons, especially in spring and summer. Forcing the model with measured tree transpiration, HR_B decreased during spring and summer, while the contribution of the underlying rock layer to tree transpiration was threefold that estimated using HR_R-based model. The average water content of the bulk surface soil layer was very low, reaching 0.06 in the driest summers while showing little diurnal dynamics; however, concentrating water in roughly estimated rhizosphere volume, produced rhizosphere water content appreciably higher ($\approx$0.16), and much more dynamic. Predicted HR_R dominated evapotranspiration (60% - 65%) in dry springs and summers reaching 80% of tree transpiration. Most importantly, the proposed rhizosphere-HR model correctly predicts the diurnal dynamics of tree transpiration year-round, and the grass transpiration in its active spring period. Eco-hydrological models operating at sub-daily scale should consider partitioning the soil to rhizosphere volume, thus allowing both diagnostic and prognostic estimates of diurnal biosphere-atmosphere mass and energy exchanges.

1. Introduction

Trees in semi-arid ecosystems often survive prolonged droughts extracting water from deeper soil, fractured cemented horizons or rock layers, where water stored during wet seasons supplies transpiration in dry seasons (David et al., 2013; N. Nadezhdina et al., 2015; Sperry and Love, 2015; Fan et al., 2017; Montaldo et al., 2021). In such climates, where thin soils are overlaying fractured bedrocks, forest ecosystems may obtain 70–90% of the water used in evapotranspiration (*ET*) from rock water storage (McCole and Stern, 2007; Breshears et al., 2009; Schwinning, 2010; Estrada-Medina et al., 2013; Rempe and Dietrich, 2018; Montaldo et al., 2021). In these water-limited conditions,

hydraulic redistribution (HR) through tree roots plays a key role in sustaining dry season transpiration by transferring water upward from the moist, deep layer into the dry surface soil (hydraulic lift, HL) (Brooks et al., 2002; Domec et al., 2010; N. Neumann and Cardon, 2012; Prieto et al., 2012; Barron-Gafford et al., 2017; Montaldo et al., 2020, 2021). During periods in which the deeper soil is not saturated, HR following rains reverses, moving water through roots from the wet surface soil into deeper, drier layers (hydraulic descent, HD). Thus, in wet seasons, HD supplements the infiltration process in recharging storage in deeper layers (Hultine et al., 2003; Scott et al., 2008; Fu et al., 2016), available in part through HL for ET in dry seasons. It has been shown that, in a typical heterogeneous water-limited Mediterranean

ecosystem, where trees clumps are surrounded by mostly seasonal grass cover, water uptake and HR by tree roots in the underlying rock layer is not only essential for tree survival during prolonged summer droughts, but is necessary to supply grass transpiration and sustain its physiological activity during its active season, spring (Montaldo et al., 2021).

Ecohydrological models need to represent these hydraulic transfer processes accurately. In ecohydrological models, HR is commonly estimated based on the bulk soil water potential gradient between surface and deep root zone soil layers (Ryel et al., 2002; Lee et al., 2005; Zheng and Wang, 2007; Yan and Dickinson, 2014; Yu and D'Odorico, 2014, 2015; Gou et al., 2018), neglecting the millimeter-scale spatial heterogeneity of water content introduced by tree roots and their associated rhizosphere, a heterogeneity that can greatly affect HL and its estimates in dry conditions (Carminati, 2012). The rhizosphere is the volume of soil enveloping roots and thus strongly affected by root functioning (Kuzyakov and Razavi, 2019). The physical, chemical and biological properties in the rhizosphere are different to the soil properties more distant from roots (Carminati et al., 2010). The spatial heterogeneity of water content introduced by the rhizosphere depends on the density of roots per soil volume. Based on neutron tomography and imaging of radioactive isotopes (Moradi et al., 2011; Kuzyakov and Razavi, 2019), rhizosphere water content can be much higher than a short distance from root surfaces when the bulk soil is dry. The volumetric water content can decrease from near saturation ($\approx$ 0.35–0.4) at the soil-root interface to level unavailable for plant uptake ($\approx$ 0.05–0.1) only 4 mm away (Moradi et al., 2011). Hence, although the average water content of the bulk surface soil layer is low in dry conditions, the water content of the rhizosphere can be much higher, requiring particular attention for accurate modeling of water flux in the surface soil during dry seasons, as has been shown in a laboratory experiment (Carminati, 2012).

In wet seasons, characterized by hydraulic descent, the water content of rhizosphere and bulk surface soil are similar (Carminati, 2012). However, in dry seasons, characterized mostly by HL, neglecting the difference in water content between the rhizosphere and the bulk soil in the surface layer may misestimate HR. Two main issues are: 1) when the soil water potential gradient is prescribed between the average water potential of the dry, bulk surface soil layer and the wetter deep layer (Yu and D'Odorico, 2014; Gou et al., 2018), upward water flux could be overestimated because the gradient would be higher than that actually driving the flux between the less dry rhizosphere and the deep layer; 2) focusing on sub-daily HR dynamics, the nocturnal recharge of the surface soil layer from deeper water source typically accounts for the diurnal water uptake from the surface layer (Domec et al., 2010), but the variation of the bulk soil average moisture produced by HR at sub-daily resolution is lower than that of the rhizosphere with its smaller volume, potentially affecting the diurnal pattern of water uptake. Misestimates of HR will result in poor prediction of the amounts of water uptake by tree roots from both surface and deep layers and, therefore, transpiration, and errors in the diurnal pattern of HR will affect diurnal predictions of stomatal conductance, and thus energy balance and photosynthesis.

We propose a new model for predicting 1) water uptake by tree roots from the fractured rock sublayer in this study and, in general, from any deeper soil medium, and 2) HR between the sublayer and surface soil, accounting for the heterogeneity in surface soil moisture caused by the rhizosphere, and for its effect on modeling ecosystem water balance at a diurnal scale. We base this on existing ecohydrologic model (Montaldo et al., 2008, 2013), which couples a land surface model (LSM) based on the widely used force-restore method (Noilhan and Planton 1989) and a vegetation dynamic model (VDM) based on the carbon assimilation approach of Cayrol et al. (2000) and Nouvellon et al. (2000); the model considers tree, grass, and bare soil components. The case study is a typical Mediterranean ecosystem in Sardinia (Detto et al., 2006; Montaldo et al., 2008, 2013, 2020), where wild olives and seasonal grass species grow on thin surface soil layer overlaying a fractured rock sublayer, and for which a long-term dataset of micrometeorological, tree transpiration, and soil water content measurements is available, and

were HR by tree roots supports the transpiration of both wild-olive clumps and surrounding grass (Montaldo et al., 2021). The proposed approach includes hydraulic redistribution, the tree root rhizosphere water balance, and the water balance of the rocky sub-layer. We demonstrated the importance of including the tree root rhizosphere and its water balance for predictions of HR and diurnal transpiration in ecohydrological modeling.

2. Methods

2.1. The ecohydrologic model with the rhizosphere water balance component

The ecohydrologic model (WR) of Montaldo et al. (2008) is based principally on coupling a land surface model (LSM; Noilhan and Planton 1989), which predicts the soil water balance and the energy balance among the soil, vegetation and atmosphere, and a vegetation dynamic model (VDM; Cayrol et al., 2000; Nouvellon et al., 2000; Montaldo et al., 2005; Fig. 1). The WR distinguishes three land cover components: tree, grass and bare soil. The purpose of the model coupling is to obtain grass and tree leaf area index (LAI) dynamics at daily resolution from the VDM to use as input, based on which the LSM computes energy and water partitioning between soil and vegetation at half-hourly time scale. The soil water balance of WR includes a surface soil layer [predicted using the force-restore approach of Noilhan and Planton (1989), as revised by Montaldo and Albertson (2001)] and a root zone soil layer. Details of the WR model are published in Montaldo et al. (2005, 2008) and Montaldo et al. (2013), with parameters defined in Table 1. Here, we improve on this formulation introducing HR, water balance of the rhizosphere, and the water balance of the rocky sub-layer (Fig. 2), which impacts ET and LAI computations. The model code is written in Matlab, and its first version was developed in Montaldo and Albertson (2001), which included the LSM for a single vegetation component. Later, the first version of the VDM for grass was coupled to the LSM (Montaldo et al., 2005), and the LSM + VDM model version was further revised to include three land cover components (Montaldo et al., 2008). Model meteorological inputs are precipitation, air temperature, wind velocity, incoming shortwave radiation, air relative humidity, and photosynthetically active radiation (Fig. 1). Model parameter inputs are in Table 1. Following we detail the revisions introduced to the WR model.

2.1.1. The land surface model

Following Montaldo et al. (2021) approach, developed for a daily resolution soil water balance, we partition the root zone into two layers, a surface soil layer and a fractured rock sublayer extending to the depth of sinker tree roots (Fig. 2), expressing their water balances as:

$$\frac{d\theta_{sl}}{dt} = \frac{1}{d_{sl}}\left[I - f_{bs}E_{bs} - f_{v,t}\xi_t E_{t,rh} - f_{v,g}\xi_{g,rh}E_{g,rh} - f_{v,g}\left(1-\xi_{g,rh}\right)E_{g,nrh} - E_w - D_r - HR\right]$$

(1)

and

$$\frac{d\theta_{fr}}{dt} = \frac{1}{d_{fr}}\left[D_r - f_{v,t}(1-\xi_t)E_{t,fr} + HR - L_e\right],$$

(2)

where θ_{sl} is soil moisture of the surface layer, θ_{fr} is moisture of the underlying fractured rock layer, d_{sl} and d_{fr} are the respective depths of these layers, I is infiltration rate, D_r is the rate of drainage out of the bottom of the surface root zone, HR is hydraulic redistribution, represented as a vertical flux through tree roots between the underlying substrate and the surface soil layer (positive when downward), L_e is leakage below the tips of sinker roots in the rock sublayer, E_{bs} is bare soil evaporation, $E_{t,rh}$ is tree transpiration from the surface layer, partially controlled by the moisture in the rhizosphere volume of the surface soil layer (θ_{rh}), $E_{t,fr}$ is tree transpiration from the fractured rock layer, $E_{g,rh}$ and $E_{g,nrh}$ are the rates of grass transpiration with roots partitioned
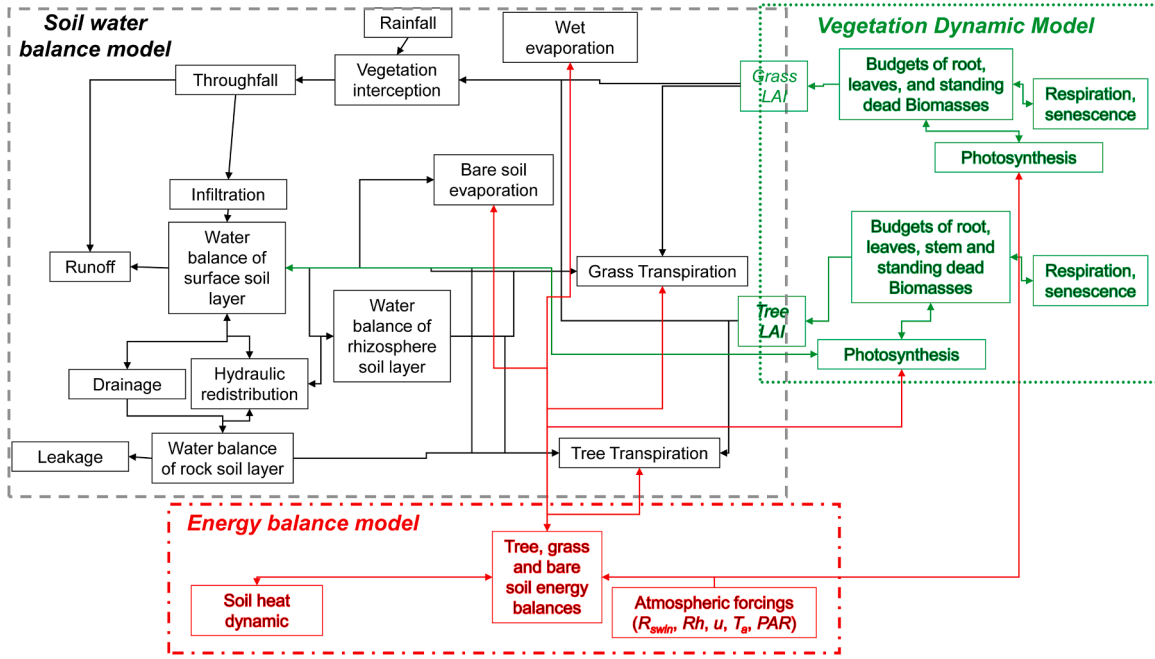
Fig. 1. WR model structure with the three main components, soil water balance, energy balance and vegetation dynamic (*LAI*: leaf area index; R_{swin}: shortwave incoming radiation; *Rh*: relative humidity; *u*: wind velocity; T_a: air temperature; *PAR*: photosynthetically active radiation).

between the rhizosphere of tree root and the rest of the surface soil layer, respectively, through $\xi_{g,rh}$, the fraction of grass root water uptake from the rhizosphere volume of tree roots, E_w is wet canopy evaporation, ξ_t is the fraction of tree root water uptake from the surface soil layer, $f_{v,t}$ is the fraction of tree cover, $f_{v,g}$ is the fraction of grass cover, and f_{bs} (=1-$f_{v,t}$ -$f_{v,g}$) is the fraction of bare soil.

The evapotranspiration, *ET*, is given by the sum of the four evapotranspiration components, bare soil evaporation, tree transpiration (which is given by the sum of $E_{t,rh}$ and $E_{t,fr}$), grass transpiration (which is given by the sum of $E_{g,rh}$ and $E_{g,nrh}$) and wet canopy evaporation. As in the original Noilhan and Planton (1989) model, the throughfall rate is modeled through a balance equation of the intercepted water by the canopy reservoir (its capacity is a function of the *LAI*), which produces throughfall when the reservoir is saturated. E_w was set to the rainfall interception (Noilhan and Planton, 1989). The infiltration is estimated using an infiltration excess mechanism (Montaldo et al., 2008), based on the Philip's infiltration equation (Philip, 1957). In the unsaturated soil the Clapp and Hornberger (1978) relationships are used to describe the non-linear dependencies of volumetric soil moisture and hydraulic conductivity (*k*) on the matric potential (ψ).

Both D_r and L_e are estimated using the unit head gradient assumption (Albertson and Kiely, 2001), so that a gravitational drainage is predicted from the surficial root zone layer and the deep fractured rock layer below the tips of the sinker roots, defining the maximum depth of the physiologically relevant rock strata (Table 2). The D_r balances with *HR*, which can be both downward (hydraulic descent, HD) and upward (hydraulic lift, HL) depending on the soil water potential gradient between surface and deep layers, and it is computed based on Ryel et al. (2002) and Yu and D'Odorico (2014), revising so it uses the soil water potential of the tree root rhizosphere, ψ_{rh}, instead of the average soil water potential of the bulk surface soil layer:

$$HR = R_e C_{rmax} \left(\psi_{fr} - \psi_{rh} \right) f_{v,t} D_{tran}, \tag{3}$$

where C_{rmax} is the maximum root hydraulic conductance of the root system, D_{tran} is a factor reducing water movement among layers by roots while the plant is transpiring, which was assumed to be 1.0 during the night when transpiration was minimal and 0.0 during the day (radiation > 0; Ryel et al., 2002; Fu et al., 2016), and R_e is a factor reducing root

hydraulic conductance and accounting for soil water limitation with decreasing soil moisture, given by (Ryel et al., 2002; Yu and D'Odorico, 2015):

$$R_e = \frac{1}{1 + \frac{max(\psi_{fr}, \psi_{rh})^{\zeta_R}}{\psi_{50}}}, \tag{4}$$

with ψ_{fr} the soil water potential of the underlying active rocky layer, ζ_R is an empirical parameter, ψ_{50} is the soil water potential where soil-root conductance is reduced by 50% (= 1 MPa, Ryel et al., 2002). We emphasize that this revises Ryel et al. (2002) and Yu and D'Odorico (2015) expression of R_e, using ψ_{rh} instead of the bulk soil water potential of the root zone. ψ_{rh} is estimated from θ_{rh} using the Clapp and Hornberger (1978) relationship, and θ_{rh} is predicted from the soil water balance of the rhizosphere:

$$\frac{d\theta_{rh}}{dt} = \frac{1}{d_{sl}} (I - D_r) - \frac{1}{d_{rh}} \left(f_{v,t} \xi_t E_{t,rh} + f_{v,g} \xi_{g,rh} E_{g,rh} + HR \right), \tag{5}$$

where d_{rh} is the depth of the rhizospheres in the d_{sl} soil depth. $E_{t,rh}$, $E_{t,fr}$, $E_{g,rh}$, and $E_{g,nrh}$ are estimated based on the Penman-Monteith equation (Brutsaert, 1982; Montaldo et al., 2008) for each plant functional type (PFT, e.g. tree and grass). The canopy resistance, r_c, accounting for environmental stresses, are estimated following Montaldo et al. (2008) for each PFT, using a typical Jarvis (1976) approach:

$$r_c = \frac{r_{s,min}}{LAI[f_1(\theta)f_2(T_a)f_3(VPD)f_4(R_{swin})]^{-1}}, \tag{6}$$

where $r_{s,min}$ is the minimum stomatal resistance, f_1, f_2, f_3 and f_4 are stress functions of soil moisture, air temperature (T_a), and vapor pressure deficit (*VPD*), and the shortwave incoming radiation (R_{swin}). Note that r_c is different for the grass and tree covers because $r_{s,min}$, *LAI*, $f_2(T_a)$ and $f_3(VPD)$ are different for each PFT (see Montaldo et al., 2008), and f_1 differs between the two PFTs and soil moisture control. In general, f_1 is a linear function of soil moisture:

Table 1
WR Model parameters (VDM-LSM model) for the Orroli site.

Parameter	Description	Value* grass	WV
LSM-VDM parameters			
$r_{s,min}$ [s m^{-1}]	minimum stomatal resistance	80	500
T_{min} [°K]	minimum temperature	272.15	268.15
T_{opt} [°K]	optimal temperature	295.15	278.15
T_{max} [°K]	maximum temperature	313.15	318.15
$\theta_{wp,sl}$ [-]	wilting point in the bulk surface soil layer	*0.10*	*0.08*
$\theta_{lim,sl}$ [-]	limiting soil moisture for vegetation in the bulk surface soil layer	0.18	0.18
$\theta_{wp,rh}$ [-]	wilting point in the rhizosphere volume	0.12	0.13
$\theta_{lim,rh}$ [-]	limiting soil moisture for vegetation in the rhizosphere volume	0.19	0.19
ω [KPa^{-1}]	slope of the f_3 relation	0.6	0.6
$\theta_{wp,fr}$ [-]	wilting point in the underlying fracture rock layer		0.08
$\theta_{lim,fr}$ [-]	limiting soil moisture for vegetation in the underlying fracture rock layer		0.18
$\xi_{g,rh}$	fraction of grass root water uptake in the tree root rhizosphere	0.1	
ξ_t	fraction of tree root water uptake from the surface soil layer	0.8	
Only VDM parameters			
c_l [m^2 gDM^{-1}]	Specific leaf areas of the green biomass in growing season	0.01	0.005
c_d [m^2 gDM^{-1}]	Specific leaf areas of the dead biomass	0.001	0.005
k_e [-]	PAR extinction coefficient	0.5	0.5
ξ_a [-]	Parameter controlling allocation to leaves	0.6	0.55
ξ_s [-]	Parameter controlling allocation to stem	0.1	0.1
ξ_r [-]	Parameter controlling allocation to roots	0.4	0.35
Ω [-]	Allocation parameter	0.8	0.8
m_a [d^{-1}]	Maintenance respiration coefficients for aboveground biomass	0.032	0.0019
g_a [-]	Growth respiration coefficients for aboveground biomass	0.32	0.76
m_r [d^{-1}]	maintenance respiration coefficients for root biomass	0.007	0.002
g_r [-]	growth respiration coefficients for root biomass	0.1	0.1
Q_{10} [-]	Temperature coefficient in the respiration process	2.5	1.5
d_a [d^{-1}]	death rate of aboveground biomass	0.023	0.0045
d_r [d^{-1}]	death rate of root biomass	0.005	0.005
k_a [d^{-1}]	rate of standing biomass pushed down	0.01	0.35
Only LSM parameters			
$z_{om,v}$ [m]	Vegetation momentum roughness length	0.05	0.5
$z_{ov,v}$ [m]	Vegetation water vapor roughness length	z_{om}/7.4	z_{om}/2.5
$z_{om,bs}$ [m]	Bare soil momentum roughness length	0.015	
$z_{ov,bs}$ [m]	Bare soil water vapor roughness length	z_{om}/10	
θ_s [-]	saturated soil moisture	0.53	
b [-]	slope of the retention curve	4	
$k_{s,sl}$ [m/s]	saturated hydraulic conductivity in the surficial root zone	5×10^{-6}	
$\sim\psi_s\sim$ [m]	air entry suction head	0.70	
$k_{s,fr}$ [m/s]	saturated hydraulic conductivity in the active fractured rock	5×10^{-4}	
b_{rh} [-]	slope of the retention curve in the tree root rhizosphere	5	
C_{rmax} [mm/MPa/h]	maximum root hydraulic conductance of the active root system	1.5×10^{-6}	
ζ_R	Empirical parameter of Eq. (4)	2	
d_{rh} [m]	depth of the tree root rhizosphere in the surficial root zone	0.014	
d_{sl} [m]	Surficial root zone depth	0.15	
d_{fr} [m]	Root zone depth of the active fractured rock	2	

* Two values for vegetation parameters are those of the grass and woody vegetation (WV).

$$f_1 = \begin{cases} 0 & if\ \theta \leq \theta_{wp} \\ \dfrac{\theta - \theta_{wp}}{\theta_{lim} - \theta_{wp}} & if\ \theta_{wp} < \theta < \theta_{lim}, \\ 1 & if\ \theta \geq \theta_{lim} \end{cases} \tag{7}$$

where θ_{lim} and θ_{wp} depend on the type of vegetation (e.g., Larcher, 1995; Eagleson, 2002; Table 1), while θ soil moisture contributors are θ_{sl} for $E_{g,nrh}$, θ_{fr} for $E_{t,fr}$, and θ_{rh} for $E_{t,rh}$ and $E_{g,rh}$. In water-limited ecosystems, soil moisture contribution is a key term of the canopy resistance, which is also used by the VDM for photosynthesis computation. The soil water balance model for the root zone can include a soil sublayer instead of the root-accessible fractured rock sublayer based on the same approach, but would require different parameter values. The expressions for $f_2(T_a)$, $f_3(VPD)$ and $f_4(R_{swin})$ are provided in Table 2.

The aerodynamic resistances are estimated as function of wind velocity through the transfer coefficient for water vapor, C_E (Garratt, 1999), according to the Monin-Obukhov similarity theory. C_E and the heat transfer coefficient (C_H, used in sensible heat flux estimates) account for atmosphere stability (Garratt, 1999), with the flux profile functions for stable and unstable conditions (Garratt, 1999; Montaldo et al., 2008).

Finally, the actual rate of bare soil evaporation is determined by (Montaldo et al., 2008):

$$E_{bs} = \alpha(\theta_{sl})PE, \tag{8}$$

where *PE* is the potential evaporation estimated by the Penman equation (e.g., Brutsaert, 1982, equations 10.15, 10.16 and 10.19), and $\alpha(\theta_{sl})$ is a rate-limiting function, estimated by the polynomial function of Parlange et al. (1999).

The state of surface temperature is estimated through the force-restore method (Noilhan and Planton, 1989; Montaldo and Albertson, 2001). Equations for surface temperature and three components (sensible heat flux, *H*, soil heat flux, *G,* and the net radiation, R_n) of the energy balance are the same as Noilhan and Planton (1989) and are reported in Table 2. They are applied separately for each land cover component (i.e. seasonal grass patches, evergreen tree clumps, and bare soil), so that the model predicts the energy balance distinctly for each land cover component.

2.1.2. The vegetation dynamic model

The VDM computes change in biomass over time from the difference between the rates of biomass production (photosynthesis) and loss, such as occur through respiration and senescence (e.g., Larcher, 1995; Cayrol et al., 2000). The VDM distinguishes woody vegetation (WV) and grass components, and is derived by Montaldo et al. (2005; 2008) from the Nouvellon et al. (2000) model.

In the VDM of WV, four separate biomass states (compartments) are tracked (green leaves, stems, living roots, and standing dead), while the VDM of the grass cover distinguishes only three of these biomass compartments (green leaves, roots, and senesced aboveground components; Table S.1). Model equations are in Table S.1 and parameters in Table 1. Leaf area index is estimated from the biomass through linear relationships (Nouvellon et al., 2000; Arora, 2003; Montaldo et al., 2005, 2008; Table S.1).

The key term of the VDM, the photosynthesis, P_g, is computed using the approach of Montaldo et al. (2005), which includes the canopy resistance estimated through (6), linking P_g to soil moisture. Hence, P_g accounts for contributions of two water sources: the surface root zone, and the fractured-rock sublayer down to the reach of tree roots. Details on the estimates of the VDM terms are provided in Montaldo et al. (2008).

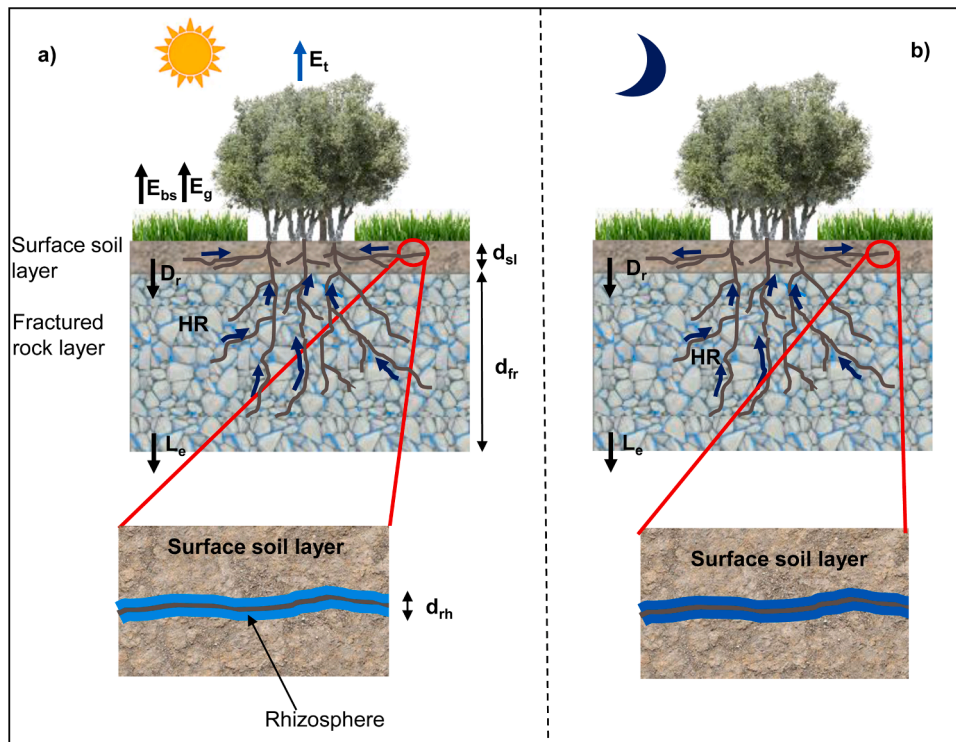The VDM provides estimates of daily values of leaf biomass and, thus,

Fig. 2. Diurnal (a) and nocturnal (b) soil water balance and hydraulic redistribution scheme, with a qualitative depiction of the rhizosphere in the surface soil layer zone in a dry day, conditions characterized by hydraulic lift exclusively (no hydraulic descent).

Table 2

Equations of drainage (D_r), leakage from the fractured rock sublayer below a plane marking the depth of sinker root (L_e), sensible heat flux (H), net radiation (R_n), soil heat flux (G), surface temperature (T_s), and the stress functions of air temperature (T_a) and vapor pressure deficit (VPD) of Eq. (6). Parameters are defined in Table 1.

Equations

Drainage

$$D_r = k_{s,sl}\left(\frac{sl}{\theta_s}\right)^{2b+3}$$

$$L_e = k_{s,fr}\left(\frac{\theta_{fr}}{\theta_s}\right)^{2b+3}$$

Stress functions of T_a, and VPD of Eq. (6)

$$f_2(T_a) = \begin{cases} 0 & \text{for } T_a \leq T_{a,min} \text{ and } T_a > T_{a,max} \\ 1 - \dfrac{T_{a,opt} - T_a}{T_{a,opt} - T_{a,min}} & \text{for } T_{a,min} < T_a < T_{a,opt} \\ 1 & \text{for } T_{a,opt} \leq T_a \leq T_{a,max} \end{cases}$$

$$f_3(VPD) = 1 - \omega\log(VPD)$$

$$f_4(R_{swin}) = \frac{R_{swin}(1000 + k_p)}{1000(R_{swin} + k_p)}$$

where R_{swin} is the shortwave incoming radiation and k_p equals 1 W/m^2 (Li et al., 2013)

Sensible heat flux

$H = \rho_a c_p C_H u(T_s - T_a)$,

with C_H the heat transfer coefficient

Net radiation

$R_n = R_{swin}(1 - \alpha) + \varepsilon(R_{lwin} - \sigma T_s^4)$,

with R_{swin}, and longwave incoming ration, R_{lwin}, estimated based on equation 6.10 of Brutsaert (1982), α albedo, ε emissivity and σ the Stefan-Boltzmann constant

Soil heat flux

$G = R_n$-H-LE

Surface temperature

$$\frac{dT_s}{dt} = C_T G - \frac{2\pi}{\tau}(T_s - T_a),$$

with T_2 the mean T_s value over one day τ, and C_T the soil thermal coefficient

$$\frac{dT_2}{dt} = \frac{1}{\tau}(T_s - T_2)$$

LAI of the WV and grass, in-turn used by the LSM to estimate evapotranspiration, energy flux, rainfall interception and the soil water content in the root-zone at a half-hour time step (Fig. 1). The LSM provides soil moisture and aerodynamic resistances to the VDM (Fig. 1).

2.1.3. Simplified model version for transpiration modeling

To assess the effect of detailing the rhizosphere-based HR on the accuracy of estimating transpiration at diurnal resolution, we compared the proposed model, which we designate as with-rhizosphere, or WR, with a no-rhizosphere, NR, version of the model that does not include Eq. (5), and uses a bulk surface soil water content in Eqs. (1)-(4). In other words, NR uses ψ_{sl}, the average soil water potential of the surface layer, as is common in ecohydrologic modeling (e.g., Ryel et al., 2002; Yu and D'Odorico, 2015) instead of ψ_{rh}. As consequences, in eqn. (1) tree transpiration from the surface layer is controlled by θ_{sl} (i.e. it is $E_{t,sl}$ instead of $E_{t,rh}$), and the grass transpiration contribution does not include water uptake from the tree root rhizosphere (i.e. it is $E_{g,nrh}$ only). We run NR (1) using the same parameters of the proposed model with rhizosphere and (2) recalibrating model parameters (designated NR-cal) forcing bulk surface soil moisture, transpiration and evapotranspiration to match the measured values.

2.2. The sardinia case study and the available data

The Orroli field site is located in east-central Sardinia (39° 41′ 12. 57″ N, 9° 16′ 30. 34″ E, 500 m a. s. l.; details in Detto et al., 2006; Montaldo et al., 2008, 2013), where an eddy covariance-based micrometeorological tower was installed in May 2003. The landscape is a patchy mixture of primarily wild-olive tree clumps forming canopy cover over ~33% of the tower footprint area, ~ 1.5 km^2 on a gently sloping (~3° from NW to SE) plateau, while inter-clump zones are covered by herbaceous and grass species during high moisture periods, becoming dry bare soil surface during the rainless summer months. The dominant trees species is wild olive in patches ranging in height 3.5–4.5 m, with scattered 6–7 m tall emergent individuals of cork oak (*Quercus*

suber), and shorter shrubs (*Asparagus acutifolius* and *Rubus ulmifolius*); vines (*Crataegus azarolus* and *Smilax aspera*) often climb the trees.

The climate at the flux site is maritime Mediterranean, with a mean annual precipitation (1922–2018) of 612 mm (historical precipitation data from a nearby station at 4 km). Mean annual air temperature (T_a) is 14.6 °C, with mean July T_a of 23.7 °C. The soil ranges 0–50 cm in depth, averaging 17 cm ± 6 cm (standard deviation, SD) above a fractured basalt, thus quickly plunging into water-limited conditions during the rainless summer (Detto et al., 2006; Montaldo et al., 2008). The soil is silt loam (19% sand, 76% silt, 5% clay) with a bulk density of 1.38 g/cm^3, and a porosity of 53%. We estimated a depth-equivalent of the rhizospheres of 14 mm from the soil depth (less 10% accounting for rock content), and assuming a ratio of 0.09 between the two depths. This ratio was estimated considering a root length density of 0.5 cm/cm^3 (olive trees; Masmoudi-Charfi et al., 2011), multiplied by rhizosphere cross sectional area of a root of mean diameter of 1 mm and a rhizosphere extension of 2 mm (Carminati et al., 2010; Kuzyakov and Razavi, 2019).

An extended monitoring was carried out from May 2003 to September 2018, during which micrometeorological, soil moisture, and vegetation dynamics measurements were conducted. Seven frequency domain reflectometer probes (FDR, Campbell Scientific Model CS-616) were inserted in the soil close to the tower (3.3–5.5 m away) to estimate moisture (θ) in the thin soil layer (Montaldo et al., 2008). FDR calibration (θ=2.324–6.801 τ+6.431 τ^2–1.815τ^3, where τ is the output period ranging from $0.8 \cdot 10^{-3}$ s to $1.6 \cdot 10^{-3}$ s) was made using 15 periodic gravimetric water content samples taken over a wide range of θ (0.08 - 0.52 m^3 m^{-3}) near the probes, and along the soil profile.

Three-dimensional time series sampling of wind velocity, temperature, and CO_2 and water vapor concentration at 10 Hz were averaged over 30 min intervals. These data were used to estimate *ET* and sensible heat flux based on the standard eddy-covariance method (Baldocchi, 2003). The measurements were made with a Campbell Scientific CSAT-3 tri-axial sonic anemometer, and a Licor-7500 CO_2/H_2O infrared gas analyzer, positioned adjacent to each other at the top of the 10 m tall tower. The effect of the gentle slope of the plateau was removed by utilizing the conventional planar fit method, and the Webb-Pearman-Leuning adjustment was applied (Detto et al., 2006).

A Vaisala HMP45 sensor was used to measure T_a and relative humidity (*Rh*). Two infrared transducers, IRTS-P (Apogee Instrument, accuracy of 0.3 °C) were used to measure the surface temperature (T_s [°C]) of the different land cover components. The incoming and outgoing shortwave and longwave radiation components used to derive R_{net} [W m^{-2}], were measured with a CNR-1 (Kipp & Zonen) integral radiometer with a hemispherical field of view, positioned at 10 m. The photosynthetically active radiation (*PAR* [mmol m^{-2} d^{-1}]) was measured with the LI-190 Quantum Sensor (Licor). Soil heat flux was measured at two different locations close to the tower, one in an open patch (4 m from the tower) and one under a tree canopy of wild olive (5.5 m from the tower), with thermopile plates, HFT3 (REBS), buried at 8 cm below the soil surface. Two thermocouples (per plate) were buried at 2 and 6 cm, and one frequency domain reflectometer probe per plate was buried horizontally at 5 cm, as needed to estimate changes in the stored energy above the plates (see HFT3 instruction manual edited by Campbell Sci.)

Sap flow was monitored using Granier-type heat dissipation sensors (Granier, 1987). Sap flux sensors measure the temperature differential (ΔT, recorded in mV) between the paired heated and unheated probes (Granier, 1987), and J_s xylem water flux is given by:

$$J_s = 119 \cdot 10^{-6} \left(\frac{\Delta T_{max} - \Delta T}{\Delta T} \right)^{1.231} \quad (9)$$

where ΔT_{max} is the maximum temperature differential at which sap flux is zero (Granier, 1987), and it was calculated each day distinctly. The ΔT_{max} values for baselining were selected with Baseliner (Oishi et al., 2016), which uses a joint occurrence for two hours of zero *VPD* (thus

ensuring no water loss to the atmosphere) and a small coefficient of variation of ΔT (thus ensuring that recharge was completed). This approach ensures that nighttime flux is quantified. However, we note that a pulse of predawn flux occurs on a number of days, representing a small fraction (averaging 8%) of the daily flux. We have no physiological explanation for the pulse; the pulse may reflect the time in which, once the stemwood is recharged with water, both the thermal conductivity of the wood, and the temperature difference between the heated sensor and the air, are high, producing the appearance of a slow but noticeable flux (Steppe et al., 2010; Vergeynst et al., 2014; Hölttä et al., 2015). Nevertheless, scaling the flux to ground-based transpiration (see below) and comparing to energy balance-based estimate obtained at a wild olive clump near the eddy covariance tower, showed a good agreement, suggesting that the effect of this pulse was negligible, and that calibrating the sensors was not necessary (Montaldo et al., 2020).

We measured the diameter (Ø, in cm, at height of 0.4 m aboveground) of 1615 trees in 21 clumps (all stems $\geq$1 cm) within the footprint, in the two prevailing wind directions from the tower [mistral (northwest) and sirocco (southeast); Montaldo and Oren, 2016]. Based on these we selected nine trees of diameters representing the range of these found on the footprint to determine sapwood depth from tree cores (after Oishi et al., 2008). We installed sap flux sensors at the height of 40 cm in the trunks of 33 trees. Each pair of sensors was 20 mm in length and the heated element received a constant power of 0.2 W. ΔT for each sensor pair was measured at 1 s intervals, averaged over 30 min and stored on three CR3000 dataloggers (Campbell Scientific, Logan, UT, USA). Time series of the sap flux measurements were not continuous due to interruptions in the power supply, downtime for maintenance, and sensor failure. Thus, of these 33 sensors, we selected 11 sensors, which satisfied the following conditions (Montaldo et al., 2020): 1) the sensor produced clean and reasonable patterns in the data for more than a quarter of measurement days, 2) the sensor had operated over periods in which daily mean θ ranged from at least 0.08 to 0.25, and 3) the sensor had operated over periods in which the half-hourly vapor pressure deficit ranged from <0.5 kPa to >4.0 kPa. The selected 11 monitored trees represented eight of the 21 clumps, and the tree size distribution within the footprint (Ø ranged 5.0–13.0 cm, with mean of 8.3 cm and SD of 2.1 cm, similar [$p = 0.12$] to that of the 1615 trees [mean Ø 7.0 cm and SD of 2.8 cm]). Given the small diameter of most stems, radial pattern was not anticipated nor quantified. The sapwood area of trees with Ø $\geq$ 5.0 cm, the minimum reasonable diameter for our heat dissipation probe, represent 90.6% of the total sapwood area (see further details in Montaldo et al., 2020). Sap flux was measured from September 2011 to August 2018.

In scaling sap-flux to the eddy-covariance footprint, we used data from 21 clumps selected within the prevailing directions in the footprint (including the 15 clumps in which sap flux sensors were installed, and additional six clumps farther from the tower). In each clump we estimated the ratio A_{sw}/A_g (A_{sw} is the total tree sapwood area of the clump, and A_g is the clump's ground area, represented by its canopy projection). Sap flux, J_s, was scaled to tree transpiration within the clump area, E_t^{SF}, with A_{sw}/A_g (Oren et al., 1998):

$$E_t^{SF} = J_s \frac{A_{sw}}{A_g} \quad (10)$$

Because clumps are very dense, we anticipated and found differences in flux rates depending on the position of stems in the clump, with stems at the center and northern edges of clumps transpiring less than stems at the southern edge; scaling sap flux accounted for the proportion of A_{sw}/A_g of each clump in these categories.

2.3. Comparisons and statistical data analysis

Data were analyzed at hourly, daily, monthly, seasonal and yearly time scales. For annual computations, we use the hydrologic year

beginning in Sardinia in September, the end of a typical dry summer. An index of wetness (*P/PE*, precipitation/potential evaporation) was used for distinguishing seasonal meteorological conditions.

Model goodness-of-fit was evaluated comparing modeling results with observations and using the following statistics: mean (μ), standard deviation (SD), coefficient of variation (CV), mean error (me), root mean square error (rmse), correlation coefficient (ρ), and mean ratio (R$_μ$).

3. Results

3.1. Model validation and performance

Over the 15-year long record, annual rainfall ranged 817 mm/y to 448 mm/y, with large interannual variability (CV = 0.16, Fig. 3a); the mean of 629 mm/y (SD = 102 mm/y) is similar to the historical mean annual precipitation beginning 1922. Potential evaporation ranged 1505 mm/y to 980 mm/y, with a mean of 1179 mm/y (SD = 147 mm/y, CV = 0.12, Fig. 3a). The rainfall regime is a typical Mediterranean maritime, with maximum in winter months (in average ≈ 3 mm/d in November) and minimum in summer months (near zero in July, Fig. 3b). The interannual variability reflects a large variation in monthly precipitation of all months (Fig. 3b), with CV > 0.5, increasing to ≈ 1.7 in July and August. The potential evaporation regime is nearly in opposite
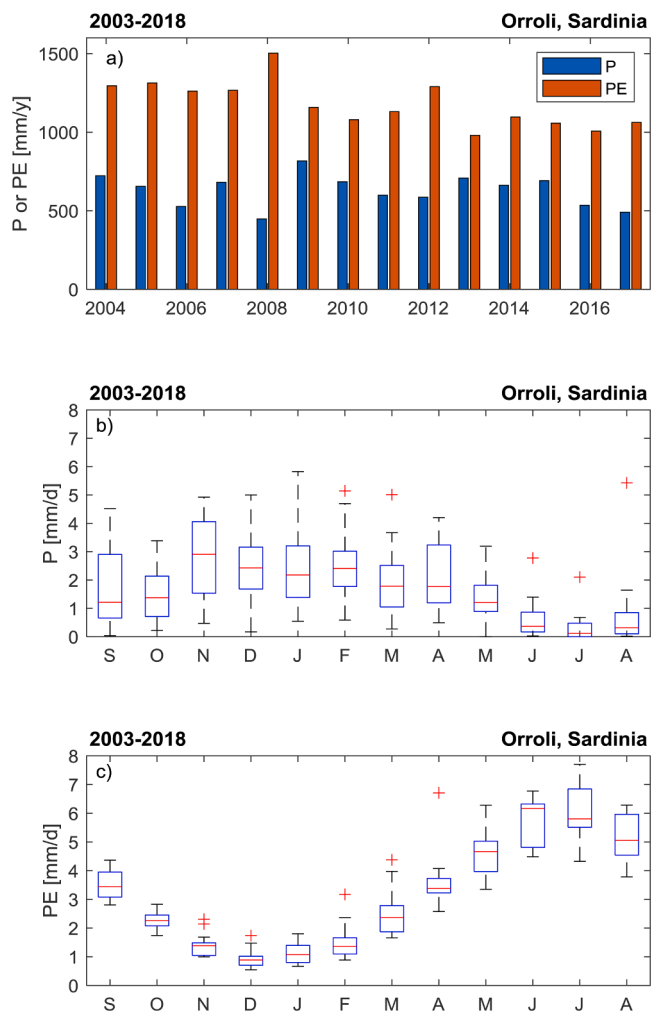

Fig. 3. (a) Yearly precipitation (P) and potential evaporation (PE). Monthly regimes of (b) precipitation and (c) potential evaporation (in each box, red line indicates the median, the box and whiskers represent quartiles, and outliers are depicted individually). (For interpretation of the references to colour in this figure legend, the reader is referred to the web version of this article.)

phase to the rainfall regime (Fig. 3c), reaching a maximum of ≈ 6 mm/d in July and minimum of ≈ 1 mm/d in December, yet was less variable for a given month with CV < 0.40, reaching a minimum of 0.15 in summer months.

Here, we first evaluate the predictions of the WR version of the model. The WR soil water balance model predicted soil moisture well when compared with $θ_{sl}$ observations over the 15-year long record (Fig. 4; results from statistical test of model performance are given in Table 3), showing the model predictions following the strong seasonal pattern of soil moisture, ranging ≈ 0.50 in wet months to ≈ 0.08 at the end of summer (Fig. 4). Predicted soil moisture responded to rain dynamics, resulting in strong seasonal correlation with precipitation (correlation coefficient, ρ = 0.79). Predicted soil moisture in tree root rhizosphere was higher than $θ_{sl}$ during dry seasons (> 0.15), while $θ_{fr}$ showed lower temporal variability (Fig. 4b) ranging ≈ 0.31 (usually at the end of winter) to ≈ 0.21 (usually at autumn), and was less correlated with seasonal precipitation dynamics (ρ = 0.37). However, inter-annual $θ_{fr}$ dynamics were explained by that of precipitation (ρ = 0.76), with $θ_{fr}$ reaching lowest values of ≈0.21 at the end of 2008 and 2017 (Fig. 4b), after the driest hydrologic years (< 500 mm) of the 15-year long record (Fig. 3).

The WR model predicted *ET* reasonably well (rmse = 0.51 mm/d, ratio of the sums = 0.883, Table 3), with *ET* ranging from ≈ 3.5 mm/d in spring to less than ≈ 1 mm/d in summer (Fig. 5b). The observed E_t from scaled sap-flux measurements was also well-predicted during the shorter monitoring period (Fig. 5a; rmse= 0.295 mm/d; ratio of the means = 0.875, Table 3). The other two modules of the model, the vegetation dynamic module and the energy balance module, previously calibrated (Montaldo et al., 2008, 2013), allowed reasonable predictions of additional key ecohydrologic variables (e.g., net radiation, sensible heat flux, *LAI*). Model parameters are in Table 1, and statistical evaluation of model performance are in Table 3.

Hydraulic lift was predicted by WR to occur mostly in spring and summer, reaching 0.9 - 1.0 mm/d late May and early June (Fig. 5b). In dry conditions, values of HR were similar to tree transpiration values. In wet seasons the predicted hydraulic descent reached 0.8 mm/d (mainly in autumn, Fig. 5b). Focusing on dynamics at sub-daily scale, HR peaked at ≈ 20:30, later than the peak of the tree transpiration at ≈ 10:30, which in turn was slightly earlier than the peak of *PE* (Fig. 6). Due to water uptake by tree roots from the surface layer during daytime, soil moisture decreased to a minimum in the late afternoon. During the nighttime, HR recharged the soil, increasing soil moisture to a maximum in the morning. Both $θ_{sl}$ and $θ_{rh}$ followed this hourly dynamic, but $θ_{sl}$ (averaging ≈ 0.10) was lower than the predicted $θ_{rh}$, and varied little (between 0.101 and 0.097) compared with the variation predicted for the rhizosphere (between 0.180 and 0.147). Because of the low soil moisture content of d_{sl}, the soil water potential was very low (≈ −3.0 MPa), nearing typical wilting point values, conditions that would have greatly impede water uptake from the surface soil. In contrast, rhizosphere soil was estimated to have enough water to keep the water potential above –0.8 MPa, sufficiently high to permit tree roots to extract water in support of transpiration (Fig. 6).

HR contributed to *ET* more as the index of wetness decreased in spring and summer [*HR/ET*=1. 612–1. 600 P/PE$^{0. 128}$, R^2=0.81, *p*<0.001; Fig. 7], up to 60–65% of *ET* during the driest summers (*P/PE*<0.05), and up to 50% during the driest springs (*P/PE*≈ 0.10). While in winter HR contribution was small, in autumn HR contribution to *ET* was greater, averaging 13% (Fig. 7), and reaching up to 19%. Because tree transpiration rates are lower, HR contributed a larger fraction of tree transpiration, again increasing with decreasing *P/PE* [*HR/E_t*=0.985–0.867 P/PE$^{0.512}$, R^2=0.80, *p*<0.0001; Fig. 7], becoming particularly high in dry summers (*PE/P* < 0.20) in which HR was 80–85% of E_t (Fig. 7). Note that, in Fig. 7, lines are fitted only to spring and summer data; winter data were excluded because *HR/ET* and *HR/E_t* were very low and uncertain, and autumn data because HR contributions can be high even while the seasonal wetness index is high due to
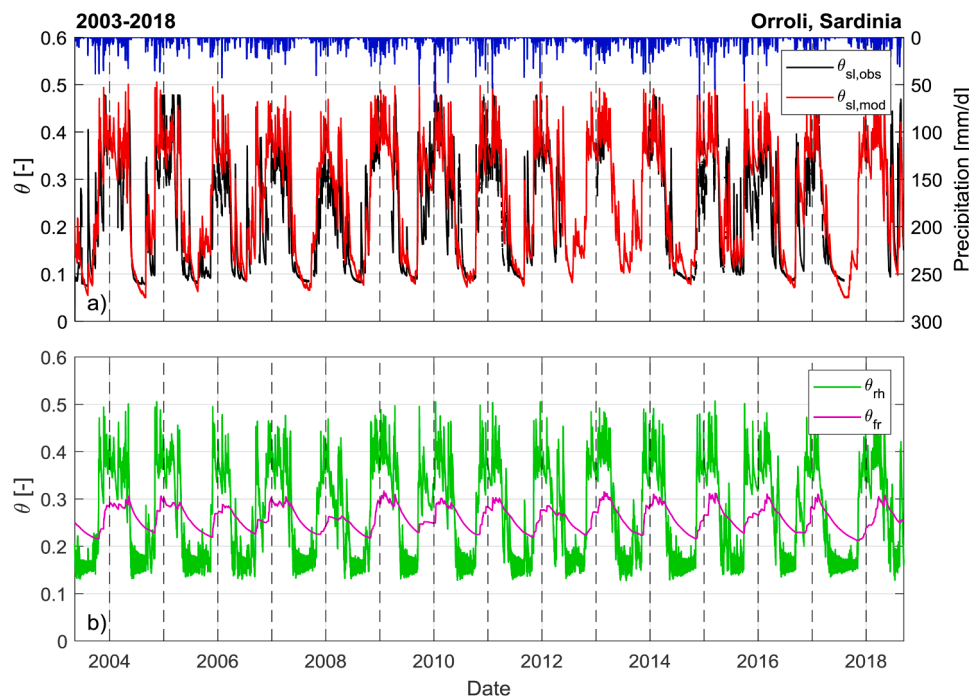
Fig. 4. Using WR, daily values of (a) the observed and modeled soil moisture of the surface soil layer (θ_{sl}), and (b) the predicted moisture of the underlying active rocky layer (θ_{fr}) and the tree root rhizosphere (θ_{rh}). Measured precipitation (in blue) is shown in (a) panel. (For interpretation of the references to colour in this figure legend, the reader is referred to the web version of this article.)

Table 3
Statistics of WR model performance (μ = mean, SD = standard deviation, me = mean error, rmse= root mean square error, ρ = correlation coefficient, R_μ = mean ratio) for soil moisture of the surface root zone (θ_{sl}), evapotranspiration (ET), tree transpiration (E_t), net radiation (R_n), and sensible heat flux (H).

Variable	μ	SD	|me|	rmse	ρ	R_μ
θ_{sl}	0.219	0.119	0.021	0.058	0.892	1.096
ET	1.074 mm/d	0.651 mm/d	0.125 mm/d	0.506 mm/d	0.692	0.883
E_t	0.633 mm/d	0.307 mm/d	0.079 mm/d	0.295 mm/d	0.501	0.875
R_n	3.398 mm/d	1.889 mm/d	0.004 mm/d	1.359 mm/d	0.759	0.999
H	2.412 mm/d	1.441 mm/d	0.252 mm/d	1.145 mm/d	0.731	1.104

occasional dry soil conditions in early autumn, the start of the hydrologic year in Sardinia. Finally, HR contribution to annual ET averaged 22% (reaching 29%), and HR contribution to annual E_t was even greater, averaging 47%, and reaching up to 57%.

3.2. Comparison of the proposed rhizosphere versus common bulk-soil modeling of transpiration

We compared transpiration predictions based on the proposed WR model, with predictions based on the NR and the NR-cal models (Fig. 8a-c). The modeled tree transpiration based on each model version during two dry days of July 2015 is shown, including the contributions from the surface layer ($E_{t,surf}$, which is $E_{t,rh}$ in WR), the fractured rock layer ($E_{t,fr}$), and the HR transfer of water from the fractured rock recharging the surface layer (Fig. 8d). Not accounting for the rhizosphere water balance, but using the same parameters of WR, the NR model predicted low tree transpiration (Fig. 8a) driven by low θ_{sl} and small contribution from the surface layer (Fig. 6). Owing to moisture limitation in the bulk surface soil, and the (non-linear) effect of soil moisture on stomatal conductance, NR-predicted canopy conductance peak was about a quarter of the ~0.0056 m/s calculated based on sapflux measurements

(Fig. 8e), but the timing of peak daily transpiration and, thus, conductance was similar to the observed (Fig. 8f; $P = 0.263$, Mann-Whitney test for difference between the distribution of peak daily E_t time versus observations; $n = 96$).

Calibrating NR, to match observed values of daily tree transpiration while forcing the bulk surface soil moisture to match the observations, the fraction of tree root water uptake from the fractured rock layer (=1-ξ_t) increased to 52% (from 20% in NR and WR, Table 1), HR decreased (C_{rmax} in eqn. (3) was set to one-tenth that of NR and WR), and, although conductance peak increased to 0.0033 m/s, it remained lower than the observed (Fig. 8e). Moreover, the diurnal pattern of E_t predicted by NR-cal was substantially different from the observed pattern ($P < 0.001$), peaking in the afternoon (~ 15:00 in 52% of days and ~ 13:00 in 32% of days) instead of ~ 11:00 (Fig. 8b). The diurnal pattern of E_t based on NR-cal reflects that of VPD together with conductance remaining higher in the afternoon (Fig. 8e), due to unchanging soil moisture.

Introducing the rhizosphere component into the model eliminated the large underestimation observed in the transpiration predicted with NR, and the smaller underestimation but large delay in peak time predicted with NR-cal. Indeed, the diurnal pattern and amounts of transpiration and canopy conductance based on the revised WR model matched that from observation (Fig. 8c, e). Predicted diurnal E_t peak using the proposed WR model occurred at a similar time of the day of the observed E_t peak (10:30–11:00; Fig. 8f; $P > 0.125$ for the distributions of timing of peak transpiration versus observation).

Predicted HR by NR was almost constant during the nightime, in contrast to HR predicted by WR, showing dynamic water flux between the fractured rock and the surface layer (Fig. 8a,c). The difference in the HR dynamics reflects a feedback with the highly variable of θ_{rh} predicted by WR as opposed for the nearly invariable θ_{sl} predicted by NR (Fig. 6). The diurnal pattern of E_t based on the proposed WR, suggested a maximum hourly uptake rate of rock water of 0.02 mm/h (Fig. 8c), which was the same in NR (Fig. 8a).

We calculated the mean daily E_t obtained from the surface soil layer and from the underlying fractured rock in the four seasons based on each model configuration (Fig. 9). Note that the total amount of E_t based on
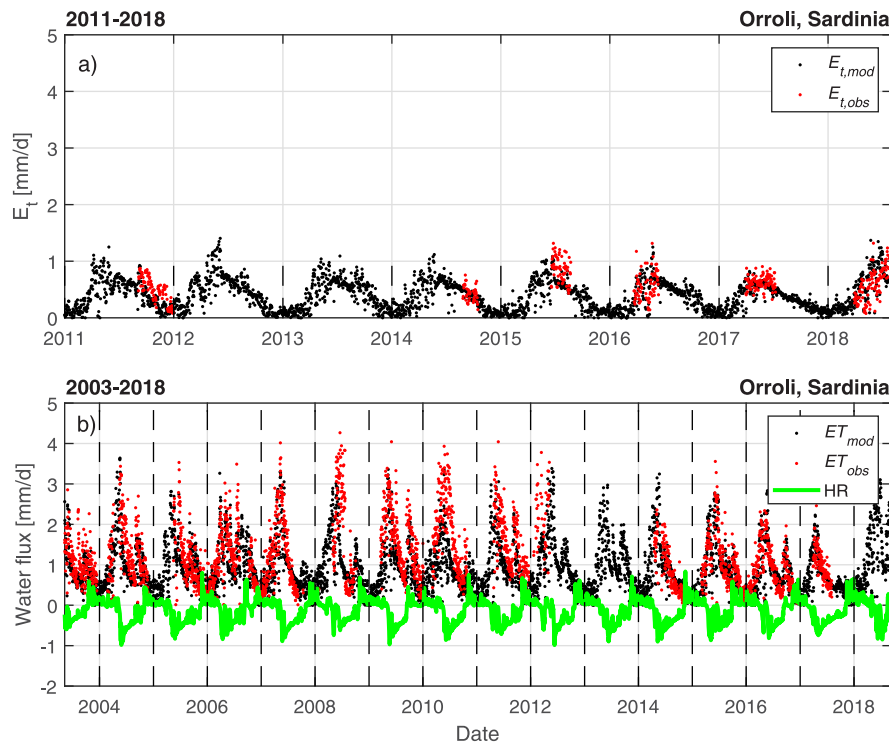
2011-2018 **Orroli, Sardinia**

2003-2018 **Orroli, Sardinia**

Fig. 5. Using WR, observation and model predictions of (a) daily tree transpiration (E_t), and b) daily evapotraspiration (*ET*) and estimated hydraulic redistribution (HR) predictions. Negative values of HR represent hydraulic descent while positive values represent hydraulic lift.
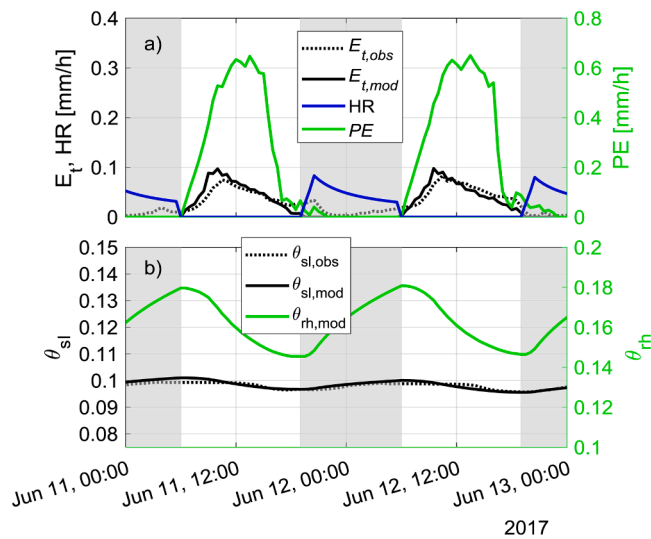

Fig. 6. Using WR, during two dry days of June 2017 (a) observed and predicted hourly tree transpiration (E_t) potential evaporation (*PE*) and hydraulic redistribution (HR), and (b) observed and predicted hourly soil moisture of the surface soil layer (θ_{sl}), and predicted soil moisture of the tree-root rhizosphere (θ_{rh}). The gray zones mark nighttime hours. (For interpretation of the references to colour in this figure legend, the reader is referred to the web version of this article.)

NR-cal was forced to match the observed. E_t was underestimated using the NR configuration, up to 23% in spring and 56% in summer compared to WR predictions (Fig. 9), and up to 19% in spring and 62% in summer compared to the fewer sapflux-based observations (complete data of only two springs and one summer were available). The contribution of the tree root water uptake from the surface soil decreased from WR-estimated 0.49 mm/d to NR-estimated 0.36 mm/d during spring
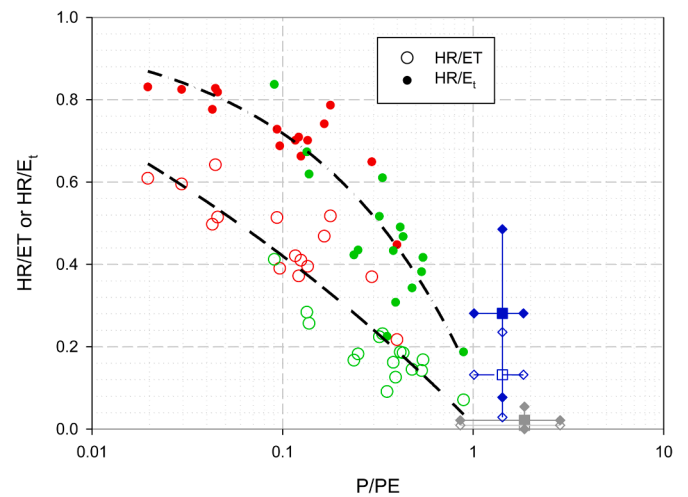

Fig. 7. Using WR, the seasonal contributions of hydraulic redistribution (HR) to evapotranspiration (ET) and tree transpiration (E_t) versus the index of wetness (P/PE, precipitation/ potential evaporation). For spring and summer data are plotted in green and red circles, respectively; for autumn and winter seasonal means are plotted in blue and gray squares (solid lines and diamonds are mean±SD). Regression lines are for spring and summer data (dash line: HR/ET=1.612–1.600 P/PE$^{0.128}$, R^2=0.81, *p*<0.001; dash dot line: HR/E_t=0.985–0.867 P/PE$^{0.512}$, R^2=0.80, *p*<0.0001). (For interpretation of the references to colour in this figure legend, the reader is referred to the web version of this article.)

(Fig. 9c); an even greater difference, 0.40 mm/d versus 0.12 mm/d, was predicted in summer (Fig. 9d). Following calibration, NR-cal predicted the contribution of direct water uptake by tree roots from the underlying fractured rock to increase from 0.11 mm/d (using NR) to 0.26 mm/d (using NR-cal) during spring, and from 0.12 mm/d (using NR) to 0.46 mm/d (using NR-cal) during summer (Fig. 9).
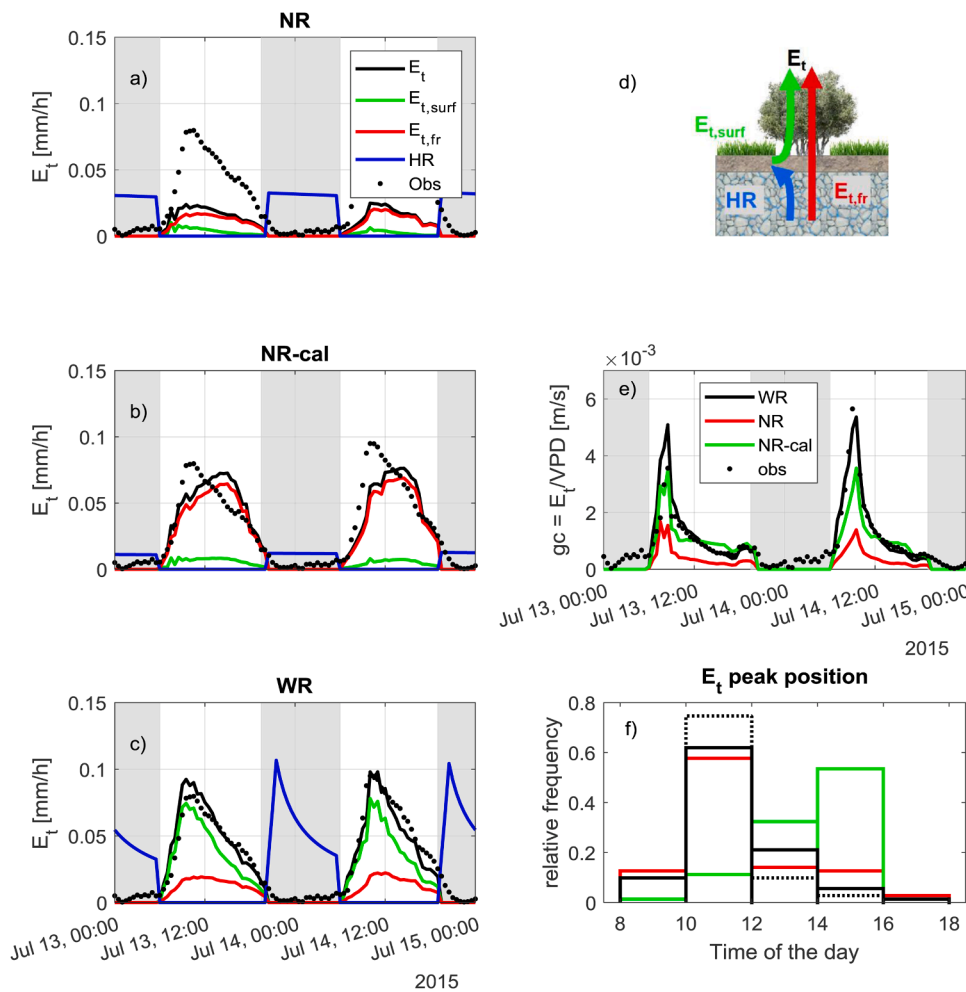
Fig. 8. Comparisons of hourly observed and predicted tree transpirations (E_t) and their contributions (from surface layer, $E_{t,surf}$, from fractured rocky layer, E_{fr}, and hydraulic redistribution, HR, defined in (d)) using (a) the model without θ_{rh} but with same parameters ("NR"), (b) the model without θ_{rh} and recalibrated parameters ("NR-cal"), and (c) the proposed model with θ_{rh} soil moisture of the tree rhizosphere ("WR"), at the Orroli site. (e): comparison of hourly predicted canopy conductance values using the three model versions with observed values; (f): comparison of the relative frequencies of the E_t peak position using the three model versions with those observed using scaled sapflux ($n = 196$ days). In panels a, b, c and e the gray zones mark nighttime hours. (For interpretation of the references to colour in this figure legend, the reader is referred to the web version of this article.)

Predictions of grass transpiration (E_g) using NR-cal were mostly lower than predictions based on the proposed WR for surface soil moisture lower than 0.2 (Fig. 10). In particular, spring E_g predictions using NR-cal averaged -0.39 mm/d for $\theta_{sl} = 0.12$–0.13, with peaks of $<$ -0.85 mm/d compared to E_g predictions using WR (Fig. 10). This is because in the NR-cal version grass was supplied by the drier bulk surface soil water, not using the hydraulically distributed rhizosphere moisture, facilitated by tree roots.

4. Discussion

Resistances to flow in the soil-plant-atmosphere pathway operate against water potential gradients, slowing down the throughput of water. Buffering the resistances and facilitating daytime transpiration are two well-studied processes. The recharge of plant tissue capacitance, which allows water, extracted from moderately moist soil at a slow throughput over many nighttime hours, to concentrate nearer to the ports of gas-exchange (Waring and Running 1978; Phillips et al., 2004; Ward et al., 2013; Domec et al., 2020), thus made available for higher rates of transpiration in the early morning hours when VPD is low, boosting water-use efficiency (Tognetti et al., 2004) and growth efficiency (Oren et al., 1987). And the hydraulic redistribution (HR), typically the prolonged nighttime absorption and lifting of water from deeper, moist ground layers, and deposition in the surficial, dry soil layer, where the concentration of fine roots is higher, later withdrawn against lesser resistance in support of transpiration (Domec et al., 2010; R.B. Neumann and Cardon, 2012). Accounting for the first process, hereafter plant storage capacity (PSC), allows more reasonable estimates

of coarse-scale water-use, and better matching of the dynamics of transpiration and water uptake – the latter estimated, for example, based on sapflux measurements (Phillips et al., 2004; Ward et al., 2013). Accounting for PSC produces diurnal patterns of gas-exchange and water relations similar to observed (Hartzell et al., 2017; Preisler et al., press).

Accounting for the second process, HR, has been shown to produce a reasonable matching of water uptake and transpiration at coarse temporal scale (Fu et al., 2016; Wu et al., 2020), but the diurnal match of these fluxes is poor, especially in arid environment where the diurnal amplitude of soil moisture is very small. This study demonstrates that partitioning the bulk soil into an additional compartment, the rhizosphere, allows the physical processes of HR and water uptake to match coarse scale water uptake while also producing diurnal dynamics of uptake matching expected pattern of transpiration of trees year-round and grasses in spring, as well as soil moisture dynamics. We did not account for PSC of wild olive in this study. Low PSC is expected in species having dense wood (Hartzell et al., 2017), such as wild olive ($\sim$ 1 g/cm^3). Indeed, despite not accounting for PSC, water uptake and transpiration dynamics matched the observed when accounting for the rhizosphere (Fig. 8c), suggesting that wild olive trees rely primarily on HR to the rhizosphere (HR$_R$).

Higher PSC was proposed a property of drought avoidance species, more suitable for moist regions, while low PSC proposed a property of drought tolerance species in dry regions (Richards et al., 2013; Hartzell et al., 2017). We propose that species that are less reliant on PSC, may not only be able to accommodate lower xylem water potential without excessive cavitation (Richards et al., 2013; Hartzell et al., 2017), but may instead avoid drought effects through a greater reliance to HR$_R$.
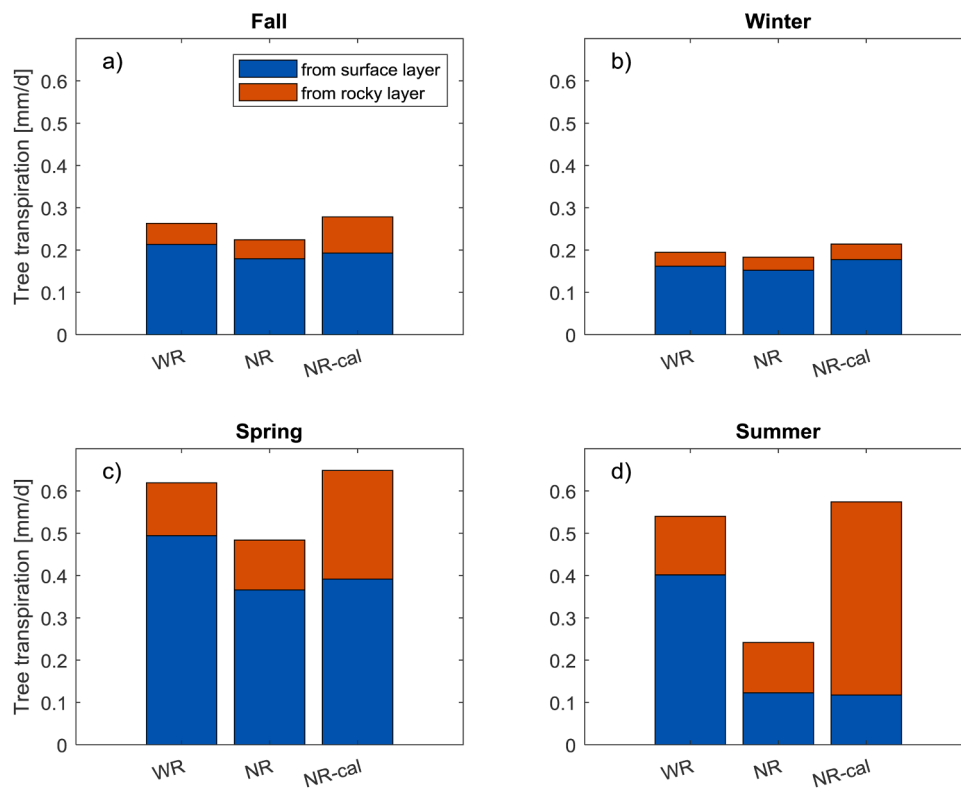
Fig. 9. The comparison of the average tree transpiration contributions (from the surface soil layer, and from the underlying fractured rock sublayer with θ_{fr} soil moisture) using the proposed model with soil moisture of the tree-root rhizosphere ("WR"), using the model without θ_{rh} but with same parameters ("NR"), and using the model without θ_{rh} and recalibrated model parameters ("NR-cal") for the four seasons at the Orroli site during the 2003–2018 period.
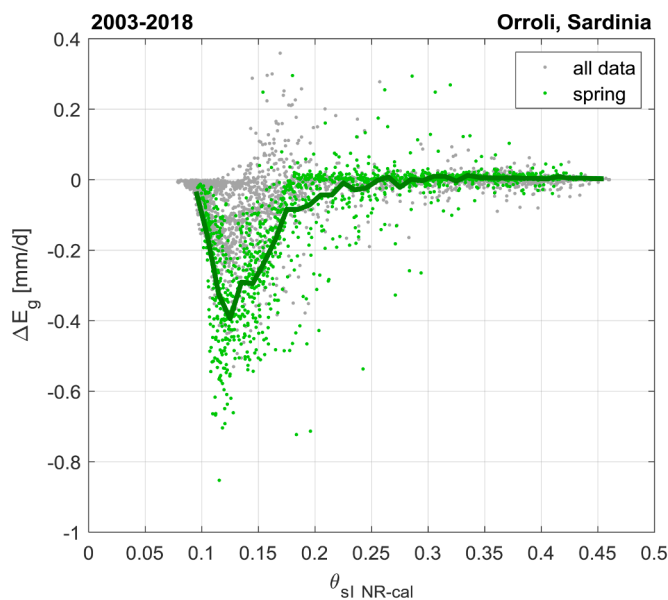

Fig. 10. Differences in grass transpiration predictions using the NR-cal model and the WR model (ΔE_g) for the range of bulk surface soil moisture predicted by NR-cal ($\theta_{sl\ NR-cal}$; in thick dark green line the mean of spring data). (For interpretation of the references to colour in this figure legend, the reader is referred to the web version of this article.)

The Sardinian site is characterized by a unimodal monthly regime of precipitation with frequent droughts in summer, typical of maritime Mediterranean precipitation regime (Montaldo and Sarigu, 2017; Corona et al., 2018; Seager et al., 2019; Fig. 3). The persistent droughts in July and August at the end of the Sardinian hydrological year,

characterized by low precipitation and high potential evaporation (Fig. 3), present challenging conditions for tree function and survival. Combined with low PSC of the wild olive, due to its high wood density, these seasonal droughts made this a case study suitable for investigating whether species in drought-prone regions must indeed rely only on their capacity to withstand low xylem water potential to overcome extreme water-limiting conditions (Richards et al., 2013; Hartzell et al., 2017).

Common to trees growing in uplands of Mediterranean basins (Schwinning, 2010; Estrada-Medina et al., 2013; Montaldo et al., 2020), wild olive trees grow on thin surface soil layer, which does not contain sufficient moisture to support tree transpiration during the dry season. Trees survive droughts using, during dry seasons, the moisture collected during wet seasons (autumn and winter) and held in soil pockets in the underlying fractured rock, into which tree roots penetrate (Estrada--Medina et al., 2013; Rempe and Dietrich, 2018; Corona and Montaldo, 2020; Montaldo et al., 2021). Indeed, both downward gravitational drainage through soil layers and hydraulic descent through tree root systems recharge deep layer during wet seasons. In this Mediterranean ecosystem characterized by heavy fall and winter precipitations (averaging 69% of annual precipitation), the simplified model estimated soil drainage to dominate over the contribution of hydraulic descent, the latter process accounting for only 6% of the annual downward flow from the surface soil layer. However, in drier ecosystems downward HR in wet periods recharged deeper layers, and was found to be essential for woody vegetation survival in the dry season (Scott et al., 2008; Lee et al., 2018). Modeling reliance on moisture obtained from fractured rock subsoil layer is consistent with observations in other Mediterranean regions as well, including a Mexican limestone quarry and a hillslope within the Northern California Coast Ranges (Estrada-Medina et al., 2013; and Rempe and Dietrich 2018). In addition to uptake of moisture in direct support of transpiration, rock moisture is hydraulically redistributed to the surface soil during the dry season (Montaldo et al., 2021). Indeed, HR was observed at the site over a drying cycle in the summer of

2018, as water taken by tree roots placed in the senesced grass-covered area surrounding tree clumps was deposited in the shallow soil under the clumps (Montaldo et al., 2021).

The inclusion of a deep soil layer is common in ecohydrologic modeling (e.g., Gerten et al., 2004; Van Der Knijff et al., 2010; Cai et al., 2014). Recognizing that the fractured rock layer underlying the thin soil functions as the deeper soil layer in such models (Montaldo et al., 2021), we modeled the underlying fractured rock reservoir and predicted its water balance at hourly time scale. The deeper layer could not be parameterized based on the properties of the actual geological profile of the fractured rock, yet the use of the *arbitrarily* parameterized layer allowed accounting for the water flux interactions between the two layers and, thus, for the hydraulic redistribution. The fractured rock layer was predicted to nearly always contain enough moisture to allow absorption (>0.22, except in autumn of 2008 and 2017, at the end of the driest hydrologic years of the observed period, Fig. 4b), presenting valuable water reservoir for tree survival during dry months.

The typically structured model with two-layer substrate of, here, soil-over-fractured rock (NR), greatly underestimated daily tree transpiration (Fig. 8a), because, although predicted soil moisture was higher than observed during dry periods (Figure S.1), it remained in the range highly limiting to stomatal conductance. Indeed, the common approach, which does not partition the surface soil into rhizosphere and bulk soil (Ryel et al., 2002; Lee et al., 2005; Yan and Dickinson, 2014; Yu and D'Odorico, 2014, 2015; Gou et al., 2018), underestimated daily E_t because it underestimated the daily peaks of HR. This approach, however, produced diurnal pattern similar to the observed, because HR, driven by the water potential gradient between the fractured rock and the surface soil (Figure S.1), raised soil moisture in the surface layer to a maximum in the morning, the diurnal period of lowest soil moisture limitation to stomatal conductance (Fig. 8). Following Yu and D'Odorico (2015), we forced the model to match the observed daily transpiration (averaged over the entire observation period), by shifting more roots into the wetter rock layer while keeping the bulk moisture of the thin surface soil similar to measured values (NR-cal). This version produced a diurnal transpiration pattern very different from the observed (Fig. 8b), reflected in transpiration peak placed in midafternoon instead of midmorning, owing to maintenance of afternoon conductance higher than observed coupled with the diurnal peak of VPD.

The fraction of tree roots in the rocky sublayer was increased from 0.20 of NR and WR versions to 0.52 in NR-cal to meet the observed transpiration demands, a high and rarely reported fraction of roots in deep rocky horizons (Zeng, 2001; Tokumoto et al., 2014; Hasenmueller et al., 2017). With more roots placed in the fractured rock layer, NR-cal achieved higher daily transpiration than NR by absorbing and *directly* transpiring more water from the fractured rock layer, in difference to NR which relied more heavily on HR (from the fractured rock into the surface layer) as the primary source of water for next day's transpiration (Fig. 8). We note, however, that, in the calibrated version, matching the measured transpiration rates despite the forced, measured, low soil moisture, by increasing the fraction of tree roots in the rocky sublayer, could only be achieved through a reduction of the maximum root hydraulic conductance in the HR estimate (equation 3; to a tenth of WR). Otherwise, in addition to increasing direct transpiration of rock moisture, high HR would have been realized, predicting higher than observed surface soil moisture, as was wrongly predicted by the NR version. The alternative, to have tree transpiration supported entirely by direct rock moisture uptake, worsen the diurnal match with observed transpiration. Thus, NR-cal failed to match the diurnal transpiration pattern, and predicted more rock moisture directly supplying transpiration, decreasing HR relative to that predicted with NR.

In contrast, introducing rhizosphere in the surface soil (WR), thus allowing the computation of hydraulic redistribution using the rhizosphere soil moisture, increased transpiration to values similar to the observed, maintained diurnal pattern of transpiration and conductance similar to the observed (Fig. 8c, e), and increased the reliance on

hydraulically redistributed water into the rhizosphere. The result of having rhizosphere was an estimated large dry season difference between the mean moisture of the bulk surface soil layer (≈ 0.08) and the rhizosphere moisture (≈ 0.16; Fig. 4 and 6), consistent with observations using neutron tomography and imaging of radioactive isotopes (Moradi et al., 2011; Kuzyakov and Razavi 2019). Moreover, the bulk soil experienced diurnal moisture amplitude smaller than the entire bulk soil of NR, but, because of prescribed high resistance to water flow between the rhizosphere volume and the bulk soil, the rhizosphere experienced a much larger amplitude, as observed in controlled experiments (Carminati et al., 2010). Within the WR framework, the diurnal soil moisture dynamics in dry periods predict nocturnal recharge of the surface soil layer equal to the diurnal water uptake from the layer, yet the diurnal variation of the bulk surface soil moisture was nearly 10-fold lower (≈ 0.004, Fig. 6b) than the variation of rhizosphere water content (≈ 0.035; Fig. 6b) owing to 10-fold greater bulk soil volume.

The larger amplitude, despite smaller potential gradient between the fractured rock moisture and the rhizosphere (Figure S.1), reflects a smaller rhizosphere volume showing a quicker rise in moisture concentration with HR, and a quicker depletion as the wetter soil near roots allows higher conductance and, thus, transpiration, despite adjusting stomatal response to require higher rhizosphere moisture for the same conductance. Indeed, when the rhizosphere water balance was included in the model, the recharging of the rhizosphere occurs over hours of no transpirational water loss (Fig. 6), and, once recharged, the available rhizosphere water is rapidly lost to the atmosphere in the morning, following by a long nighttime period of HR-facilitated rhizosphere recharge. This pattern of predicted water uptake from the underlying fractured rock, peaking in the evening, and lasting through the night (Fig. 6c), has been observed by Domec et al. (2010) and Prieto et al. (2012). Although the commonly observed pattern of conductance and transpiration (Tognetti et al., 2004; Dominguez et al., 2019; Moriana et al., 2002) was predicted by both NR and WR, only the inclusion of rhizosphere produced both correct pattern and similar quantity of transpiration (Fig. 6).

The WR-based direct transpiration of rock moisture in spring and summer was a third that predicted by NR-cal (Fig. 9). WR predicted high rates of HR (0.9–1.0 mm/d during dry summers, Fig. 5a and 6c), consistent with estimates from seasonal flux measurements during the 2014–2017 summers at the Orroli site (Montaldo et al., 2021). Predicted HR contribution to ET increased during dry springs and in summers when seasonal P/PE < 0.2 (Fig. 7), reaching highest values of 60% - 65% of *ET*, similar to observations at the site (Montaldo et al., 2021; see their Fig. 5). Moreover, the contribution of HR to tree transpiration accounted for up to 85% of E_t for similarly dry seasons. Such high contribution of HR was also observed by Schwinning (2010) in Mediterranean Jeffrey pine trees.

Predicting an accurate diurnal pattern and correct amounts of tree transpiration, ecohydrological models must properly represent the deeper rooting zone, even where the actual geological profile is a fractured rock layer containing tree roots, and include a rhizosphere compartment in HR computations of the surface layer. We demonstrated that neglecting the rhizosphere soil water balance would result in not only predicting tree transpiration poorly, but in heterogenic vegetation type, where seasonal grass surrounds tree clumps, grass transpiration may be under-predicted by as much as 0.8 mm/d (58%) in spring due to low tree roots-facilitated HR (Fig. 10). Such under-prediction during the season of maximum physiological activity and growth of grass in such climates, will frustrate predictions of carbon and energy balance by the grass component, accounting for two-thirds of the ground cover in this ecosystem. Indeed, even following the approach of Yu and D'Odorico (2015) who suggested that hydraulic lift is essential for tree-grass coexistence in savanna ecosystem, would not have provided grasses with enough moisture to function properly. Only allowing grass roots to absorb HR_R water from the rhizosphere of tree roots recovered the observed spring transpiration of grasses (Montaldo et al., 2020; 2021).

Our proposed approach aims at adding the minimal detail necessary to describe the soil-vegetation dynamic interactions well enough to match the typical soil moisture measurements and ecosystem-scale fluxes. Indeed, detailed hydraulic models (e.g., Mackay et al., 2015; Cai et al., 2018; Mackay et al., 2019) would be very difficult to parameterize, and may not improve predictions of flux dynamics over the simpler approach we proposed. Given that our goal was to keep the model practical, we opted for the simplification suggested by Ryel et al. (2002), and widely used in similar coarse-scale models (Lee et al., 2005; Zheng and Wang, 2007; Yan and Dickinson, 2014; Yu and D'Odorico, 2014, 2015; Gou et al., 2018), adding the rhizosphere in the surface soil with satisfactory results.

5. Conclusion

One hypothesis on how different evergreen species negotiate droughts posits that, species in more moist environments, weather short duration droughts through high PSC, facilitated by lower density sapwood, thus preventing low xylem water potential from developing (Richards et al., 2013). The tradeoff of this avoidance strategy is having low tolerance for very negative xylem water potential. In contrast, evergreen trees in more dry environments are characterized by high-density sapwood of low PSC. Although such wood may provide little buffer against the development of low xylem water potential, such a buffer is presumably less necessary because the xylem can tolerate a greater tension without excessive cavitation. Indeed, xylem water potential ranging from -3.5 MPa to -8.0 MPa have been observed in wild olives during the dry season (Lo Gullo and Salleo, 1988; Fernandez et al., 1997; Moriana et al., 2003). Nevertheless, the hypothesis is not consistently supported by data, and plant strategies may be more complex and context dependent (Hartzell et al., 2017). For example, *Pinus helepensis* growing in arid areas rely greatly on PSC to subsidize daily transpiration and conductance (Preisler et al., press). Similarly, this study shows that wild-olive trees, while in all likelihood allow low water potential to develop, must nevertheless rely on their rhizosphere as capacitance. This suggests that simply allowing water potential to drop, does not provide enough return in terms of water uptake from the deeper layer, and the rhizosphere storage must be recharged to meet transpirational demands. Recharging its rhizosphere, the wild-olive supports not only itself, but also the surrounding seasonal grass.

Diurnal and seasonal patterns of transpirations affect predictions of energy balance components and canopy photosynthesis from models based on conductance at diurnal scale (Arora, 2002; Zhou et al., 2014; Buckley et al., 2017). Beyond just misestimating vegetation performance, models which are unable to predict transpiration dynamics correctly, will also misestimate soil water balance predictions. Poor prediction of soil water balance will affect estimates of water yield, which, in certain seasons provide most of the water resources in semi-arid regions, affecting actual and future water resources planning and management strategies.

Declaration of Competing Interest

Acknowledgments

Supplementary materials

Supplementary material associated with this article can be found, in the online version, at doi:10.1016/j.agrformet.2021.108720.

References

Albertson, J.D., Kiely, G., 2001. On the structure of soil moisture time series in the context of Land Surface Models. J. Hydrol. 243 (1–2), 101–119.

Arora, V., 2002. Modeling vegetation as a dynamic component in soil vegetation-atmosphere transfer schemes and hydrological models. Rev. Geophys. 40 (2), 3.1–3.26.

Baldocchi, D., 2003. Assessing the eddy covariance technique for evaluating carbon dioxide exchange rates of ecosystems: past, present and future. Glob Chang. Biol. 9, 1–14.

Barron-Gafford, G.A., Sanchez-Cañete, E.P., Minor, R.L., Hendryx, S.M., Lee, E., Sutter, L. F., Tran, N., Parra, E., Colella, T., Murphy, P.C., Hamerlynck, E.P., Kumar, P., Scott, R.L., 2017. Impacts of hydraulic redistribution on grass-tree competition vs facilitation in a semi-arid savanna. New Phytol. 215 (4), 1451–1461. https://doi.org/10.1111/nph.14693.

Breshears, D.D., Myers, O.B., Barnes, F.J., 2009. Horizontal heterogeneity in the frequency of plant-available water with woodland intercanopy-canopy vegetation patch type rivals that occurring vertically by soil depth. Ecohydrology 2 (4), 503–519.

Brooks, J.R., Meinzer, F.C., Coulombe, R., Gregg, J., 2002. Hydraulic redistribution of soil water during summer drought in two contrasting Pacific Northwest coniferous forests. Tree Physiol. 22, 1107–1117.

Brutsaert, W., 1982. Evaporation into the atmosphere: theory, history, and applications. Kluwer Academic Publishers, p. 299.

Buckley, T.N., Sack, L., Farquhar, G.D., 2017. Optimal plant water economy. Plant Cell Environ. 40, 881–896.

Cai, X., Yang, Z.-.L., Xia, Y., Huang, M., Wei, H., Leung, L.R., Ek, M.B., 2014. Assessment of simulated water balance from Noah, Noah-MP, CLM, and VIC over CONUS using the NLDAS test bed. J. Geophys. Res. Atmos. 119, 13751–13770. https://doi.org/10.1002/2014JD022113.

Carminati, A., 2012. A model of root water uptake coupled with rhizosphere dynamics. Vadose Zone J. 11 https://doi.org/10.2136/vzj2011.0106.

Carminati, A., Moradi, A.B., Vetterlein, D., Vontobel, P., Lehmann, E., Weller, U., Vogel, H.- J., Oswald, S.E., 2010. Dynamics of soil water in the rhizosphere. Plant Soil 332, 163–176. https://doi.org/10.1007/s11104-010-0283-8.

Cayrol, P., Chehbouni, A., Kergoat, L., Dedieu, G., Mordelet, P., Nouvellon, Y., 2000. Grassland modeling and monitoring with SPOT-4 VEGETATION instrument during the 1997-1999 SALSA experiment. Agric. For. Meteorol. 105, 91–115.

Clapp, R.B., Hornberger, G.M., 1978. Empirical equations for some hydraulic properties. Water Resour. Res. 14, 601–604.

Corona, R., Montaldo, N., Albertson, J.D., 2018. On the role of NAO-driven interannual variability in rainfall seasonality on water resources and hydrologic design in a typical mediterranean basin. J. Hydrometeorol. 19 (3), 485–498.

Corona, R., Montaldo, N., 2020. On the transpiration of wild olives under water-limited conditions in a heterogeneous ecosystem with shallow soil over fractured rock. J. Hydrol. Hydromech. 68 (4), 338–350. https://doi.org/10.2478/johh-2020-0022, 2020.

David, T.S., Pinto, C.A., Nadezhdina, N., et al., 2013. Root functioning, tree water use and hydraulic redistribution in Quercus suber trees: a modeling approach based on root sap flow. For. Ecol. Manage. 307, 136–146.

Detto, M., Montaldo, N., Albertson, J.D., Mancini, M., Katul, G., 2006. Soil moisture and vegetation controls on evapotranspiration in a heterogeneous Mediterranean ecosystem on Sardinia, Italy. Water Resour. Res. 42 (8), 16.

Domec, J.C., King, J.S., Noormets, A., Treasure, E., Gavazzi, M.J., Sun, G., McNulty, S.G., 2010. Hydraulic redistribution of soil water by roots affects whole-stand evapotranspiration and net ecosystem carbon exchange. New Phytologist 187 (1), 171–183.

Domec, J.-.C., Berghoff, H., Way, D.A., Moshelion, M., Palmroth, S., Kets, K., Huang, C.-.W., Oren, R., 2020. Mechanisms for minimizing height-related stomatal conductance declines in tall vines. Plant Cell Environ. 42, 3121–3139. https://doi.org/10.1111/pce.13593.

Dominguez, C.M.R., Santana, V.H., Buckley, T.N., Fernández, J.E., 2019. Sensitivity of olive leaf turgor to air vapour pressure deficit correlates with diurnal maximum stomatal conductance. Agric. For. Meteorol. 272–273, 156–165.

Eagleson, P.S., 2002. Ecohydrology Darwinian Expression of Vegetation Form and Function. Cambridge University Press, New York.

Estrada-Medina, H., Graham, R.C., Allen, M.F., Jimenez-Osornio, J.J., Robles-Casolco, S., 2013. The importance of limestone bedrock and dissolution karst features on tree root distribution in northern Yucatan, Mexico. Plant Soil 362 (1–2), 37–50.

Fan, Y., Miguez-Macho, G., Jobbágy, E.G., Jackson, R.B., Otero-Casal, C., 2017. Hydrologic regulation of plant rooting depth. Proc. Natl. Acad. Sci. U.S.A. 114 (40) https://doi.org/10.1073/pnas.1712381114, 10,572–10,577.

Fernandez, J.E., Moreno, F., Giron, I.F., Blazquez, O.M., 1997. Stomatal control of water use in olive tree leaves. Plant Soil 190 (2), 179–192.

Fu, C., Wang, G., Goulden, M.L., Scott, R.L., Bible, K., Cardon, Z.G., 2016. Combined measurement and modeling of the hydrological impact of hydraulic redistribution using CLM4.5 at eight AmeriFlux sites. Hydrol. Earth System Sci. 20 (5), 2001–2018. https://doi.org/10.5194/hess-20-2001-2016.

Garratt, J.R., 1999. The Atmospheric Boundary Layer. Cambridge University Press, Cambridge.

Gerten, D., Schaphoff, S., Haberlandt, U., et al., 2004. Terrestrial vegetation and water balance – hydrological evaluation of a dynamic global vegetation model. J Hydrol (Amst) 286, 249–270.

Gou, S., Miller, G.R., Saville, C., Maxwell, R.M., Ferguson, I.M., 2018. Simulating groundwater uptake and hydraulic redistribution by Phreatophytes in a high-resolution, coupled subsurface-land surface model. Adv. Water Resour. 121, 245–262.

Granier, A., 1987. Evaluation of transpiration in a Douglas-fir stand by means of sap flow measurements. Tree Physiol. 3, 309–320.

Hartzell, S., Bartlett, M.S., Porporato, A., 2017. The role of plant water storage and hydraulic strategies in relation to soil moisture availability. Plant Soil 419, 503–521. https://doi.org/10.1007/s11104-017-3341-7.

Hasenmueller, E.A., Gu, X., Weitzman, J.N., Adams, T.S., Stinchcomb, G.E., Eissenstat, D.M., Drohan, P.J., Brantley, S.L., Kaye, J.P., 2017. Weathering of rock to regolith: the activity of deep roots in bedrock fractures. Geoderma 300, 11–31. https://doi.org/10.1016/j.geoderma.2017.03.020.

Hölttä, T., Linkosalo, T., Riikonen, A., Sevanto, S., Nikinmaa, E., 2015. An analysis of Granier sap flow method, its sensitivity to heat storage and a new approach to improve its time dynamics. Agric. For. Meteorol. 211, 2–12.

Hultine, K.H., Cable, W.L., Burgess, S.S.O., Williams, D.G., 2003. Hydraulic redistribution by deep roots of a Chihuahuan Desert phreatophyte. Tree Physiol. 23, 353–360.

Jarvis, P.G., 1976. The interpretation of the variations in leaf water potential and stomatal conductance found in canopies in the field. Phil. Trans. R. Soc. Lond., B. 273, 593–610.

Kuzyakov, Y., Razavi, B.S., 2019. Rhizosphere size and shape: temporal dynamics and spatial stationarity. Soil Biol. Biochem. 135, 343–360. https://doi.org/10.1016/j.soilbio.2019.05.011.

Larcher, W., 1995. Physiological Plant Ecology. Springer, p. 506 third edition.

Lee, J.E., Oliviera, R.S., Dawson, T.E., Fung, I., 2005. Root functioning modifies seasonal climate. Proceedings of the National Academy of Sciences, USA 102, 17576–17581.

(...) Li, S., Kang, S., Zhang, L., Li, F., Hao, X., Ortega-Farias, S., Guo, W., Jiang, X., 2013. Quantifying the combined effects of climatic, crop and soil factors on surface resistance in a maize field. J. Hydrol. (Amst) 489, 124–134. https://doi.org/10.1016/j.jhydrol.2013.03.002.

Lo Gullo, M.A., Salleo, S., 1988. Different strategies of drought resistance in three Mediterranean sclerophyllous trees growing in the same environmental conditions. New Phytol. 108, 267–276.

Masmoudi-Charfi, C., Masmoudi, M., Mechli, N.Ben, 2011. Root distribution in young Chétoui olive trees (Olea europaea L.) and agronomic applications. Adv. Hortic. Sci. 25, 112–122.

McCole, A.A., Stern, L.A., 2007. Seasonal water use patterns of Juniperus ashei on the Edwards Plateau, Texas, based on stable isotopes in water. J. Hydrol. (Amst) 342 (3–4), 238–248.

Montaldo, N., Albertson, J.D., 2001. On The Use Of The Force-Restore SVAT Model Formulation For Stratified Soils. J. Hydrometeorol. 2 (6), 571–578.

Montaldo, N., Rondena, R., Albertson, J.D., Mancini, M., 2005. Parsimonious Modeling of Vegetation Dynamics for Ecohydrologic Studies of Water-Limited Ecosystems. Water Resour. Res. 41 (10), W10416. https://doi.org/10.1029/2005WR004094.

Montaldo, N., Albertson, J.D., Mancini, M., 2008. Vegetation dynamics and soil water balance in a water-limited Mediterranean ecosystem on Sardinia, Italy. Hydrol. Earth Syst.Sci. 12, 1257–1271.

Montaldo, N., Corona, R., Albertson, J.D., 2013. On the separate effects of soil and land cover on mediterranean ecohydrology: two contrasting case studies in Sardinia, Italy. Water Resour. Res. 49, 1123–1136.

Montaldo, N., Sarigu, A., 2017. Potential links between the North Atlantic Oscillation and decreasing precipitation and runoff on a Mediterranean area. J Hydrol (Amst) 553, 419–437.

Montaldo, N., Curreli, M., Corona, R., Oren, R., 2020. Fixed and variable components of evapotranspiration in a Mediterranean wild-olive -grass landscape mosaic. Agric. For. Meteorol. 280, 107769 https://doi.org/10.1016/j.agrformet.2019.107769.

Montaldo, N., Corona, R., Curreli, M., Sirigu, S., Piroddi, L., Oren, R., 2021. Rock water as a key resource for patchy ecosystems on shallow soils: digging deep tree clumps subsidize surrounding surficial grass. Earth's Future 9. https://doi.org/10.1029/2020EF001870 e2020EF001870.

Moradi, A.B., Carminati, A., Vetterlein, D., Vontobel, P., Lehmann, E., Weller, U., Hopmans, J.W., Vogel, H.-J., Oswald, S.E., 2011. Three-dimensional visualization and quantification of water content in the rhizosphere. New Phytol. 192, 653–663.

Moriana, A., Villalobos, F.J., Fereres, E., 2002. Stomatal and photosynthetic responses of olive (Olea europaea L.) leaves to water deficits. Plant Cell Environ. 25, 395–404.

Moriana, A., Orgaz, F., Fereres, E., Pastor, M., 2003. Yield responses of a mature olive orchard to water deficits. J. Am. Soc. Horticult. Sci. 128, 425–431.

Nadezhdina, N., Ferreira, M.I., Conceicao, N., Pacheco, C.A., Hausler, M., David, T.S., 2015. Water uptake and hydraulic redistribution under a seasonal climate: long-term study in a rainfed olive orchard. Ecohydrology 8, 387–397. https://doi.org/10.1002/eco.1545.

Neumann, R.B., Cardon, Z.G., 2012. The magnitude of hydraulic redistribution by plant roots: a review and synthesis of empirical and modeling studies. New Phytologist 194, 337–352.

Noilhan, J., Planton, S., 1989. A simple parameterization of land surface processes for meteorological models. Montly. Weather Review. 117, 536–549.

Nouvellon, Y., Rambal, S., Lo Seen, D., Moran, M.S., Lhomme, J.P., Begue, A., Chehbouni, A.G., Kerr, Y., 2000. Modelling of daily fluxes of water and carbon from shortgrass steppes. Agr. Forest. Meteorol. 100 (2–3), 137–153.

Oishi, A.C., Hawthorne, D., Oren, R., 2016. Baseliner: an open-source, interactive tool for processing sap flux data from thermal dissipation probes. Software-X. https://doi.org/10.1016/j.softx.2016.07.003.

Oren, R., Waring, R.H., Stafford, S.G., Barrett, J.W., 1987. Twenty-four years of Ponderosa pine growth in relation to canopy leaf area and understory competition. Forest Sci. 33, 538–547.

Oren, R., Phillips, N., Katul, G., Ewers, B.E., Pataki, D.E., 1998. Scaling xylem sap flux and soil water balance and calculating variance: a method for partitioning water flux in forests. Ann. Des Sci. Forestieres 55 (1–2), 191–216.

Parlange, M.B., Albertson, J.D., Eichinger, W.E., Cahill, A.T., Jackson, T.J., 1999. Evaporation: use of fast response turbulence sensors, Raman lidar and passive microwave remote sensing. Vadose Zone Hydrol. edited by M. B.

Philip, J.R., 1957. The theory of infiltration: 1. The infiltration equation and its solution. Soil Sci. 83, 345–357.

Phillips, N.G., Oren, R., Licata, J., Linder, S., 2004. Time series diagnosis of tree hydraulic characteristics. Tree Physiol. 24, 879–890.

Preisler, Y., Hölttä, T., Grünzweig, J.M., Oz, I., Tatarinov, F., Ruehr, N.K., Rotenberg, E., Yakir, D., 2021. The importance of tree internal water storage under drought conditions. Tree Physiol.

Prieto, I., Armas, C., Pugnaire, F.I., 2012. Water release through plant roots: new insights into its consequences at the plant and ecosystem level. New Phytologist 193, 830–841.

Rempe, D.M., Dietrich, W.E., 2018. Direct observations of rock moisture, a hidden component of the hydrologic cycle. Proc. Natl Acad. Sci. USA 115 (11), 2664–2669.

Richards, A.E., Wright, I.J., Lenz, T.I., Zanne, A.E., 2013. Sapwood capacitance is greater in evergreen sclerophyll species growing in high compared to low-rainfall environments. Funct. Ecol. 28 (3), 734–744.

Ryel, R.J., Caldwell, M.M., Yoder, C.K., Or, D., Leffler, A.J., 2002. Hydraulic redistribution in a stand of Artemisia tridentata: evaluation of benefits to transpiration assessed with a simulation model. Oecologia 130, 173–184.

Seager, R., Osborn, T.J., Kushnir, Y., Simpson, I.R., Nakamura, J., Liu, H., 2019. Climate variability and change of mediterranean-type climates. J Clim 32 (10), 2887–2915. https://doi.org/10.1175/JCLI-D-18-0472.1.

Schwinning, S., 2010. Ecohydrology bearings - invited commentary the ecohydrology of roots in rocks. Ecohydrology 3, 238–245.

Scott, R.L., Cable, W.L., Hultine, K.R., 2008. The ecohydrologic significance of hydraulic redistribution in a semiarid savanna. Water Resour. Res. 44, W02440. https://doi.org/10.1029/2007WR006149.

Sperry, J.S., Love, D.M., 2015. What plant hydraulics can tell us about responses to climate-change droughts. New Phytologist 207, 14–27.

Steppe, K., De Pauw, D.J.W., Doody, T.M., Teskey, R.O., 2010. A comparison of sap flux density using thermal dissipation, heat pulse velocity and heat field deformation methods. Agric. For. Meteorol. 150, 1046–1056.

Tognetti, R., d'Andria, R., Morelli, G., Calandrelli, D., Fragnito, F., 2004. Irrigation effects on daily and seasonal variations of trunk sap flow and leaf water relations in olive trees. Plant Soil 263, 249–264, 1:CAS:528:DC%2BD2cXpsF2lur0%3D 10.1023/B:PLSO.0000047738.96931.91.

Tokumoto, I., Heilman, J.L., Schwinning, S., et al., 2014. Small-scale variability in water storage and plant available water in shallow, rocky soils. Plant Soil 385, 193–204. https://doi.org/10.1007/s11104-014-2224-4.

Van der Knijff, J.M., Younis, J., de Roo, A.P.J., 2010. LISFLOOD: a GIS-based distributed model for river basin scale water balance and flood simulation. Int. J. Geogr. Inf. Sci. 24, 189–212.

Vergeynst, L.L., Vandegehuchte, M.W., McGuire, M.A., Teskey, R.O., Steppe, K., 2014. Changes in stem water content influence sap flux density measurements with thermal dissipation probes. Trees-Struct. Function 28, 949–955.

Ward, E.J., Oren, R., Bell, D.M., Clark, J.S., McCarthy, H.R., Kim, H.-.S., Domec, J.-.S., 2013. The effects of elevated CO2 and nitrogen fertilization on stomatal conductance estimated from 11 years of scaled sap flux measurements at Duke FACE. Tree Physiol. 33, 135–151. https://doi.org/10.1093/treephys/tps118.

Waring, R., Running, S., 1978. Sapwood water storage: its contribution to transpiration and effect upon water conductance through the stems of old growth Douglas fir. Plant, Cell Environ. 131–140.

Wu, H., Fu, C., Wu, H., Zhang, L.L., 2020. Influence of the dry event induced hydraulic redistribution on water and carbon cycles at five AsiaFlux forest sites: a site study combining measurements and modeling. J. Hydrol. (Amst) 587, 124979.

Yan, B., Dickinson, R.E., 2014. Modeling hydraulic redistribution andecosystem response to droughts overthe Amazon basin using CommunityLand Model 4.0 (CLM4). J. Geophys. Res. Biogeosci. 119, 2130–2143. https://doi.org/10.1002/2014JG002694.

Yu, K.L., D'Odorico, P, 2014. Climate, vegetation, and soil controls on hydraulic redistribution in shallow tree roots. Adv. Water Resour. 66, 70–80.

Yu, K., D'Odorico, P., 2015. Hydraulic lift as a determinant of tree–grass coexistence on savannas. New Phytologist 207, 1038–1051. https://doi.org/10.1111/nph.13431.

Zeng, X., 2001. Global vegetation root distribution for land modeling. J. Hydrometeorol. 2 (5), 525–530.

Zhou, S., Yu, B., Huang, Y., Wang, G., 2014. The effect of vapor pressure deficit on water use efficiency at the subdaily time scale. Geophys. Res. Lett. 41, 5005–5013. https://doi.org/10.1002/2014GL060741.